Molecular and Pharmacological Evaluation of a Curcuma longa, Zingiber officinale and Allium sativum Polyherbal Formulation: Unravelling Synergistic Mechanisms against Plasmodium berghei

Iwara Iwara

arikpoeteng@unical.edu.ng

University of Calabar

Collins Igajah

University of Calabar

Katherine Eteng

University of Calabar

Godwin Igile

University of Calabar

Destiny Bisong

University of Calabar

Eyong Ubana

University of Calabar

Research Article

Keywords: Synergistic phytotherapy, Drug-resistant malaria, PfCRT-targeted inhibition, GC-MS profiling, Molecular docking, Pharmacophore modelling, Molecular dynamics simulation, Polyherbal formulation

Posted Date: November 6th, 2025

DOI: https://doi.org/10.21203/rs.3.rs-7941191/v1

Additional Declarations: No competing interests reported.

Abstract

Ethnopharmacological relevance: *Curcuma longa* (turmeric), *Zingiber officinale* (ginger), and *Allium sativum* (garlic) have a long history of use in traditional medicine, frequently formulated together as decoctions or herbal teas to manage febrile illnesses and malaria. However, despite widespread ethnomedicinal use, scientific evidence on their combined pharmacological efficacy and mechanisms remains scarce..

Aim of the study: This study aims to elucidate the synergistic molecular and pharmacological mechanisms of a *Curcuma longa*, *Zingiber officinale*, and *Allium sativum* polyherbal formulation against *Plasmodium berghei*.

Materials and methods: The ethanol-extracted polyherbal blend was analysed by GC-MS, revealing 21 bioactive compounds—oleic acid (15.84%), squalene (8.43%), ar-turmerone (6.24%), and Cholest-14-en-3-ol (4.76%) as major constituents. Molecular docking against *Plasmodium falciparum* chloroquine resistance transporter (PfCRT, PDB ID: 6UKJ) showed strong binding affinities for Cholest-14-en-3-ol and dehydroabietol (–8.4 kcal/mol), outperforming chloroquine (–5.4 kcal/mol). Pharmacophore modelling revealed critical hydrophobic and aromatic interactions. Stability of protein-ligand complexes was validated by 100 ns molecular dynamics simulations and MM/PBSA analysis (ΔG_bind = –33.13 kcal/mol). Acute oral toxicity was assessed in mice at doses up to 5000 mg/kg.

Results: The extract significantly reduced *Plasmodium berghei*-induced parasitemia by 97% on day 4, comparable to chloroquine (98%) ($p<0.05$). Haematological and liver function parameters normalised, while antioxidant markers (SOD, GPx) improved and lipid peroxidation (MDA) decreased.

Conclusion: This polyherbal formulation exhibits potent antiplasmodial and antioxidant effects, likely mediated via synergistic interactions of its phytoconstituents with parasitic molecular targets. It presents a promising ethnomedicine-inspired candidate for alternative malaria therapy, especially in drug-resistant contexts.

1.0 Introduction

Malaria remains one of the most persistent global health challenges, particularly in tropical and subtropical regions where it accounts for substantial morbidity and mortality. Over two billion individuals across 90 endemic countries and approximately 125 million travellers annually are at risk of infection (Olawale, 2023). The escalating emergence of *Plasmodium falciparum* and *P. berghei* strains resistant to conventional antimalarial agents such as chloroquine and artemisinin has significantly eroded treatment efficacy (Wicht et al., 2020). Consequently, there is a pressing need to explore new, affordable, and biologically safe therapeutic alternatives with multitarget potential.

Phytotherapy and polyherbal formulations are increasingly recognised as legitimate scientific avenues in drug discovery. Polyherbal therapies often yield synergistic effects, improving pharmacological potency,

bioavailability, and safety relative to single-plant extracts (Ouma et al., 2020; Arrey Tarkang et al., 2014). Importantly, *in vivo* validation remains indispensable for confirming these synergistic interactions under systemic physiological conditions, particularly regarding host–parasite dynamics, immunomodulation, and potential toxicity (Ochora et al., 2022).

Among the most studied medicinal botanicals, *Allium sativum* (garlic), *Zingiber officinale* (ginger), and *Curcuma longa* (turmeric) exhibit broad-spectrum pharmacological profiles that include antimicrobial, antiparasitic, anti-inflammatory, and immunomodulatory activities. Allicin from *A. sativum* disrupts parasite redox homeostasis and enhances macrophage activity (Jikah et al., 2024); gingerols and shogaols from *Z. officinale* mitigate inflammation and oxidative damage associated with parasitic infection (Patal et al., 2023); while curcumin from *C. longa* interferes with heme detoxification and parasite signalling pathways, producing significant growth inhibition (Shahrajabian et al., 2020; Ferreira, 2022). These phytoconstituents have also been shown through *in silico* and *in vitro* studies to interact with key *Plasmodium* metabolic enzymes such as dihydrofolate reductase (DHFR), lactate dehydrogenase (LDH), and cysteine proteases (Kumar et al., 2018; Bilsland et al., 2018)

Beyond malaria, this polyherbal mixture has garnered renewed scientific attention during the COVID-19 pandemic due to its therapeutic relevance in addressing overlapping symptoms. COVID-19 and malaria share several clinical features, including fever, fatigue, myalgia, and inflammatory responses (Di Gennaro et al., 2020; Hussein et al., 2020; Rayella et al., 2023). During the pandemic, formulations containing *garlic*, *ginger*, and *turmeric* were widely used across Africa and Asia as adjunct remedies to manage respiratory symptoms, reduce inflammation, and enhance immunity (Demeke et al., 2021; Jafarzadeh et al., 2021; Onyeaghala et al., 2023). Experimental studies have further demonstrated that curcumin, allicin, and gingerol possess antiviral and immunomodulatory activities that can attenuate cytokine storms and improve respiratory function (Alam et al., 2020; Liu et al., 2023). These mechanistic overlaps suggest that the combined pharmacological potential of the three botanicals extends beyond traditional use, providing a scientifically plausible rationale for exploring their synergistic effects in malaria, where similar inflammatory and immune pathways are implicated.

Evidence from preclinical studies strongly supports this direction. Ouma et al. (2020) demonstrated synergistic *in vitro* inhibition of *P. falciparum* by Kenyan polyherbal mixtures, while Arrey Tarkang et al. (2014) reported significant suppressive, curative, and prophylactic activities of the Cameroonian polyherbal product Nefang in *P. berghei*-infected mice. Similarly, Ochora et al. (2022) showed that *Securidaca longipedunculata* extract enhanced the efficacy of artemether/lumefantrine, reinforcing the viability of synergistic herbal combinations.

Accordingly, the present study investigates the synergistic anti-Plasmodium efficacy of a polyherbal formulation comprising *A. sativum*, *Z. officinale*, and *C. longa* using *P. berghei*-infected murine models, complemented by molecular modelling analyses. By integrating ethnopharmacological evidence with experimental validation, this research aims to bridge the translational gap between traditional practice

and modern pharmacology, establishing a scientifically grounded justification for *in vivo* testing of this polyherbal combination as a promising, low-cost therapeutic strategy against malaria.

2.0 Materials and Methods

2.1 Materials

Fresh rhizomes and bulbs of the plants were purchased from Ika Ika Oqua Market, Calabar, Cross River State, Nigeria. All chemicals and solvents used in this study were of analytical grade. Distilled water was prepared using a laboratory-grade stainless steel benchtop distillation unit (Ningbo Scientz Biotechnology Co., Ltd., China, Model: DZ-5). Laboratory glassware of various types and sizes, including beakers, graduated cylinders, Erlenmeyer flasks, separating funnels, and Büchner funnels, was all S Pyrex products (Corning Inc., USA). A high-performance blender (Kenwood USA, Model: Blend-X Pro BLM80) was used for homogenization. Other general-purpose tools included a retort stand with clamps, stainless steel spatulas, and corrugated cotton cloth for filtration support. Filtration was carried out using Whatman No. 1 filter paper with a 0.45 µm pore size (Cytiva, USA; Cat. No. 1001 – 125). Sample concentration was performed using a digital thermostatic water bath (Model HH-S6, XMTD Series, Zhengzhou Greatwall Scientific Industrial and Trade Co., China). Sample weights were measured using a precision digital electronic scale (Toption Group Co., Ltd., China; Model: SF-400C).

2.2 Method

2.2.1 Plant collection and preparation

The collected plants were cleaned, scrubbed of bark pills, and blended into a fine paste. For extraction, 300g of each plant's material was cold macerated in 1.5L of 98% ethanol for 48 hours. The mixtures were filtered through cheesecloth and filter paper, then concentrated under moderate heat (35–40°C) to get crude extracts. After weighing the dried extracts, they were kept in airtight containers and refrigerated at 2–8°C until use.

2.2.2 Analysis Using Gas Chromatography-Mass Spectrometry (GC-MS)

A GC-MS-QP2010 plus equipment from SHIMADZU-JAPAN was used to analyse the fractionated samples. This setup consisted of a gas chromatograph connected to a mass spectrometer and an AOC-20i autosampler. The analysis adhered to the following protocol: chromatography employed a fused silica capillary column (Rastek RT x 5 Ms; dimensions: 30 m x 0.25 mm ID x 0.25 m film thickness) coated with 95% dimethylpolysiloxane and 5% diphenyl; injection temperature was maintained at 250°C with split injection mode at 108 kPa pressure; column flow rate set at 1.58 mL/min; split ratio of 1.0; and solvent separation duration of 2.50 min. Mass spectra were acquired in the ACQ mode between 3 and 27 minutes, scanning at 1250 m/s with an event duration of 0.50 s.

2.3 *In silico* analysis

2.3.1 Molecular Docking Analysis

Fifty-six (56) bioactive compounds were identified in the polyherbal extract, and chloroquine was utilised as the ligand for docking analysis. The chemical structures of these compounds were obtained from the PubChem compound database (https://pubchem.ncbi.nlm.nih.gov). The three-dimensional structure of the target protein, Plasmodium falciparum Chloroquine Resistance Transporter (pfCRT), was retrieved from the Protein Data Bank (www.rcsb.org).

Ligand structural data files (SDF) were downloaded and utilised for molecular docking studies with pfLDH and pfCRT. Protein preparation involved the use of Chimaera 1.14, which encompassed the removal of non-essential water molecules and non-standard residues, as well as the addition of hydrogen atoms and charges. Ligands in SDF format were converted to Protein Data Bank (PDB) files with partial charge (Q) and atom type (T) (PDBQT) using PyRx, ensuring energy minimisation via an optimisation algorithm at the force field level. Docking simulations of the ligands with the protein targets were conducted using AutoDock Vina integrated within PyRx, and binding affinities were subsequently calculated. Visualisation of molecular interactions between proteins and ligands was performed using Chimera 1.14 and Discovery Studio 2020. (Johnson et al., 2022)

2.3.2 Pharmacophore modelling

During the modelling, a pharmacophore for the receptor-ligand interaction was constructed using PHASE obtained from the Schrödinger suite. Ligands exhibiting the highest binding affinity for the target protein were selected for this process. The E-pharmacophore (auto) technique was employed to generate ligand-based pharmacophore models. Parameter settings included a minimum feature distance of 2 Å, a minimum same-kind feature distance of 4 Å, and the specification of donors as vectors. The maximum allowable number of features was set to 7.

2.3.3 Molecular dynamics simulation.

Molecular dynamics simulations of the protein–ligand complex were conducted using the GROMACS software suite (version 2023.1), following standard guidelines outlined at http://www.mdtutorials.com/gmx/. The simulation workflow comprised four sequential stages: system setup, energy minimisation, equilibration, and the production MD run. Comprehensive analyses were performed to evaluate the structural and dynamic properties of the system.

Stage 1: System Setup

The initial step involved the generation of topology files for both the protein and ligand. Protein topologies were developed using a selected force field (e.g., AMBER99SB-ILDN or CHARMM36). At the same time, ligand parameters were obtained via a customised internal pipeline integrating AMBERTOOLS with ACPYPE to translate GAFF parameters into GROMACS-compatible format.

Stage 2: Energy Minimisation

To ensure a physically stable starting structure, the system underwent energy minimisation using the steepest descent algorithm. This step was essential to eliminate steric clashes and optimise the geometry, targeting a maximum force threshold below 1000 kJ/mol/nm.

Stage 3: Equilibration

The system was equilibrated in two distinct phases. An initial NVT equilibration phase was used to stabilise temperature under constant particle number and volume conditions, utilising a velocity-rescaling thermostat. Subsequently, NPT equilibration was employed to achieve pressure and density stability, applying the Parrinello–Rahman barostat. During both phases, positional restraints were maintained on heavy atoms to prevent significant deviations in the core structure.

Stage 4: Production Molecular Dynamics

Unrestrained MD simulations were performed using the leap-frog integrator, with a time step of 2 fs and a total simulation length of 100 nanoseconds. The Particle Mesh Ewald (PME) method was employed to calculate long-range electrostatic interactions, and bond lengths involving hydrogen atoms were constrained using the LINCS algorithm. Trajectories were recorded at 10 ps intervals and analysed using standard GROMACS tools and SiBioLead's proprietary MD analysis suite.

2.4 Experimental design

Group 1: Normal control (NC) treated with 0.2 mL of Placebo

Group 2: Negative control (DC) treated with 0.2 mL of Placebo

Group 3: Positive control (PC) treated with 500 mg/kg b.w of chloroquine.

Group 4: *P. berghei-infected*, treated with 400mg/kg b.w of polyherbal extract

Group 5: *P. berghei* infected, treated with 400mg/kg b.w of *A. sativum* extract

Group 6: *P. berghei* infected treated with 400mg/kg b.w of C. longa extract

Group 7: *P. berghei* infected, treated with 400mg/kg b.w of *Z. officinale extract*

2.4.1 Animal handling

The study received ethical approval (149BCM3021) from the Faculty of Basic Medical Sciences Animal Ethical Committee, University of Calabar. Forty-two albino mice weighing between 17 and 26 grams were utilised. Mice infected with the NK65 strain of chloroquine-sensitive Plasmodium berghei were obtained from the Nigerian Institute of Medical Research, Yaba, Lagos, while healthy control mice were sourced from the Department of Pharmacology, University of Calabar, Calabar. All mice were housed in the Animal House of the College of Medicine, University of Calabar, under standard laboratory conditions with ad libitum access to standard chow and water. The housing conditions included wooden cages in a

controlled environment maintained at 25°C, 50–60% relative humidity, and a 12:12 hour light-dark cycle. Before the experiment, a one-week acclimatisation period was provided for the mice to adjust to their environment, diet, and water. The distribution of animals into experimental groups followed specific protocols.

2.5 Acute toxicity study

An acute toxicity study was conducted on the polyherbal extract using the Swiss albino mice model, following Lorke's (1983) methodology. The study aimed to determine the lethal dose (LD) that would result in a 50% mortality rate (LD50) within 24 hours, which was projected to be 5000 mg/kg body weight (b.w). However, no mortalities were observed within the 24 hours.

2.6 Parasites

A chloroquine-sensitive Plasmodium berghei (ANKA) strain sourced from the National Institute of Medical Research (NIMER), Yaba, Lagos, Nigeria, was serially passaged in murine models for propagation.

2.7 Parasite inoculation

The experimental mice were injected intraperitoneally with 0.2 mL of infected blood containing approximately 1x10^7 P. berghei berghei parasitised erythrocytes, following the method of Okokon et al. (2008).

2.8 Drug Administration

The extracts and chloroquine were administered orally once daily for 4 days via gastric intubation. The administered extract doses were selected based on the acute toxicity test performed.

2.9 Biochemical assays

Estimation of serum liver enzymes (AST, ALT, ALP) was performed using test kits purchased from Agappe Diagnostics, India.

2.10 Antioxidants and Oxidative Stress Markers

Antioxidant activity and oxidative stress markers in liver tissues were evaluated using the following methodologies: reduced glutathione (GSH) as per Sedlak and Lindsay (1968), glutathione peroxidase (GPx) activity according to Rotruck et al. (1973), malondialdehyde (MDA) levels following Buege and Aust (1978), and superoxide dismutase (SOD) activity per Sun and Zigman (1978).

2.11 Data processing and interpretation

Statistical significance was determined using one-way ANOVA with post hoc Tukey test ($p < 0.05$) via Prism GraphPad 8.2.1. Data are presented as mean ± SEM (n = 6).

3.0 Result

3.1 Gas chromatography-mass spectrometry (GC-MS) analysis

Presented in Table 1 and Fig. 1 are the results of the identified compounds in the polyherbal extract, their names, percentage peak area, molecular weight, retention time, and molecular formula of the polyherbal formulation and the chromatogram, respectively. The results showed the presence of twenty-one (21) bioactive compounds in the extract. The names and compounds with the highest percentage composition were: oleic acid (15.84%), Cyclopropanecarboxylic acid, 2-methyl-2-(4-methyl-3-pentenyl (9.24), 2-Buten-1-one, 1-(2,2,5a-trimethylperhydro-1-benzoxiren-1-yl)(8.96%), Squalene(8.43%), Tumerone (6.24%), alpha.-Zingiberene (6.21%), 6-ethyl-3-octyl butyl ester(5.54%). Phytol(5.52%) and Cholest-14-en-3-ol, (3.beta.,5.alpha.)(4.76%). Other compounds were observed at trace levels with an insignificant percentage frequency

Table 1
Phytocompounds identified in the polyherbal extract of *Allium sativum*, *Curcuma longa* and *Zingiber officinale* using GC-MS

S/N	RT	Name of compound	CID number	Molecular formula	Molecular weight	Peak area %
1.	7.769	Pentandioic acid, (p-t-butylphenyl) ester	585276	$C_{15}H_{20}O_4$	264.32	1.54
2.	10.387	Amphetaminil	28615	$C_{17}H_{18}N_2$	250.34	0.49
3.	10.565	alpha.-Zingiberene	521253	$C_{15}H_{24}$	204.35	6.21
4.	10.709	(Z,E)-.alpha.-Farnesene	5362889	$C_{15}H_{24}$	204.35	1.59
5.	11.021	Cyclopropyl 4-picolyl ketone	564472	$C_{10}H_{11}NO$	161.20	1.21
6.	13.028	Ar-tumerone	558221	$C_{15}H_{20}O$	216.32	2.48
7.	13.077	Tumerone	558173	$C_{15}H_{22}O$	218.33	6.24
8.	13.493	Curlone	196216	$C_{15}H_{22}O$	218.33	3.00
9.	16.176	n-Hexadecanoic acid(palmitic acid)	985	$C_{16}H_{32}O_2$	256.42	3.84
10.	16.239	Phthalic acid, 6-ethyl-3-octyl butyl ester	6423866	$C_{22}H_{34}O_4$	362.50	5.54
11.	16.470	Methyl 2,6,10-trimethylundecanoate	102537	$C_{20}H_{40}O$	296.50	2.54
12.	17.220	7-Isopropyl-1,1,4a-trimethyl-1,2,3,4,4a,9,10,10a-octahydrophenanthrene	86869	$C_{20}H_{30}$	270.50	3.50
13.	17.549	Phytol	5280435	$C_{20}H_{40}O$	296.50	5.52
14.	17.767	Oleic Acid	445639	$C_{18}H_{34}O_2$	282.50	15.84
	17.853	Cyclopropanecarboxylic acid, 2-methyl-2-(4-methyl-3-pentenyl	549587	$C_{11}H_{18}O_2$	182.26	9.24
15.	17.927	2-Buten-1-one, 1-(2,2,5a-trimethylperhydro-1-benzoxiren-1-yl)	5365829	$C_{13}H_{20}O_2$	208.30	8.96
16.	18.785	Phosphinic acid	143409	H_3OP	49.997	1.81

RT = Retention Time

100

S/N	RT	Name of compound	CID number	Molecular formula	Molecular weight	Peak area %
17.	19.011	N-Cyclohexyl-N'-isopropylcarbodiimide	151103	$C_{10}H_{18}N_2$	166.26	2.28
18.	19.402	Cholest-14-en-3-ol, (3.beta.,5.alpha.)-	22295611	$C_{27}H_{46}O$	386.70	4.76
19.	19.741	Dehydroabietol	15586718	$C_{20}H_{30}O$	286.50	2.69
20.	20.124	Squalene	638072	$C_{30}H_{50}$	410.70	8.43
21.	20.877	Mono(2-ethylhexyl) phthalate	109265	$C_{16}H_{32}O_4$	278.34	2.29
RT = Retention Time 100						

3.2 Molecular Docking Analysis

A total of 21 bioactive compounds identified in the polyherbal formulation were subjected to molecular docking analysis against the Plasmodium falciparum Chloroquine Resistance Transporter (pfCRT; PDB ID: 6UKJ). The docking results revealed a range of binding affinities among the compounds, as indicated by their calculated Gibbs free energy (ΔG) values (Table 2). When compared to the reference drug chloroquine (ΔG = − 5.4 kcal/mol), several compounds exhibited stronger binding affinities. Notably, Cholest-14-en-3-ol, (3.beta.,5.alpha.)– and Dehydroabietol showed the highest binding energies at − 8.4 kcal/mol, followed by 7-Isopropyl-1,1,4a-trimethyl-1,2,3,4,4a,9,10,10a-octahydrophenanthrene (–8.1 kcal/mol), Ar-tumerone (–7.4 kcal/mol), and Squalene (–7.4 kcal/mol), indicating a stronger interaction with the pfCRT protein than chloroquine.

Table 2
Binding affinities(ΔG in kcal/mol) of chloroquine and Polyherbal extract compounds identified by GC-MS

S/N	Name of Compound	PubChem CID	Chloroquine resistance transporter(6UKJ)
1	n-Hexadecanoic acid (palmitic acid)	985	-5.3
2	Amphetaminil	28615	− .6.3
3	7-Isopropyl-1,1,4a-trimethyl-1,2,3,4,4a,9,10,10a-octahydrophenanthrene	86869	-8.1
4	Methyl 2,6,10-trimethylundecanoate	102537	-5.2
5	Mono(2-ethylhexyl) phthalate	109265	-6
6	Phosphinic acid	143409	-1.9
7	N-Cyclohexyl-N'-isopropylcarbodiimide	151103	-5.4
8	Curlone	196216	-6.4
9	Oleic Acid	445639	-5.5
10	alpha.-Zingiberene	521253	-6.8
11	Cyclopropanecarboxylic acid, 2-methyl-2-(4-methyl-3-pentenyl	549587	-6
12	Tumerone	558173	-7
13	Ar-tumerone	558221	-7.4
14	Cyclopropyl 4-picolyl ketone	564472	-5
15	Pentandioic acid, (p-t-butylphenyl) ester	585276	-6.1
16	Squalene	638072	-7.2
17	Phytol	5280435	-5.4
18	(Z,E)-.alpha.-Farnesene	5362889	-6
19	2-Buten-1-one, 1-(2,2,5a-trimethylperhydro-1-benzoxiren-1-yl)	5365829	-6.3
20	Phthalic acid, 6-ethyl-3-octyl butyl ester	6423866	-6.5
21	Dehydroabietol	15586718	-8.4
22	Cholest-14-en-3-ol, (3.beta.,5.alpha.)-	2295611	-8.4
23	Chloroquine	2719	-5.4

Further visualisation through 2D and 3D interaction diagrams (Fig. 2a–d) showed that the top-binding compounds, particularly Cholest-14-en-3-ol and 7-Isopropyl-1,1,4a-trimethyl-octahydrophenanthrene

formed van der Waals interactions with key residues of pfCRT. These interactions differed significantly from the binding profile of chloroquine.

3.3 Pharmacophore model studies

The pharmacophore models of the reference ligand, chloroquine and the two top-ranked ligands with the highest binding affinities for *PfCRT* are presented in Figs. 3A–C. The models revealed two principal interaction features: aromatic rings (denoted as *R*, shown in brown) and hydrophobic rings (*H*, shown in green). As illustrated in Fig. 3A, chloroquine displayed a single aromatic ring as its key interaction feature. In contrast, (Fig. 3C), 7-Isopropyl-1,1,4a-trimethyl-1,2,3,4,4a,9,10,10a-octahydrophenanthrene exhibited a more complex pharmacophore, contributing three aromatic rings, suggestive of enhanced π–π stacking potential. Meanwhile, Cholest-14-en-3-ol, (3β,5α) (Fig. 3B), featured both an aromatic ring and a hydrophobic moiety, highlighting its dual interaction capabilities. These structural attributes may contribute to their superior binding profiles compared to the standard.

3.4 Molecular Dynamics Simulation of the Cholest-14-en-3-ol, (3β,5α)-pfCRT Complex

A 100 ns molecular dynamics simulation was performed to assess the structural stability and interaction dynamics of the Cholest-14-en-3-ol, (3β,5α)-pfCRT complex. The results are illustrated in Figs. 4A–D and 5A–D.

Figure 4A depicts the RMSD trajectory of the complex throughout the simulation. An initial rise was observed within the first 20 ns, after which the system reached a plateau, maintaining RMSD values between 0.21–0.25 nm and stabilizing around 0.2 nm. These fluctuations are well within the threshold for stable protein-ligand interactions.

As shown in Fig. 4B, RMSD values were predominantly distributed between 0.1 nm and 0.26 nm, with a sharp drop beyond 0.75 nm. This distribution suggests limited conformational drift and overall structural stability.

The Rg profile (Fig. 4C) reflects the compactness of the protein. Rg values fluctuated narrowly between 1.13–1.18 nm, showing a brief initial contraction (1.12 to 1.10 nm) and remaining stable post-20 ns, indicating no significant unfolding.

Figure 4D reveals a gradual reduction in Solvent Accessible Surface Area (SASA) from ~ 50 nm² to ~ 44 nm², suggesting the complex underwent slight compaction, reducing solvent exposure during the simulation.

Additional analyses of energy profiles, secondary structure content, and hydrogen bonding (Figs. 5A–D) provided further insights into the system's stability. Figure 5A highlights the temporal changes in α-helices, β-sheets, turns, and coils. The number of structured residues ranged from 17 to 30, indicating moderate flexibility while preserving critical secondary structure elements.

The system's total energy (Fig. 5B), as computed via GROMACS, remained stable throughout the trajectory, fluctuating between − 1.25×10⁵ and − 1.35×10⁶ kJ/mol. This stability confirms a thermodynamically favourable environment.

Intermolecular hydrogen bonds (Fig. 5C) between the ligand and pfCRT ranged from 25 to 35, indicating sustained yet dynamic binding interactions. Intramolecular protein hydrogen bonds (Fig. 5D) fluctuated between 0.4 and 1, supporting structural cohesion.

3.4.1 MM/PBSA Binding Energy Analysis of the *PfCRT*–Cholest-14-en-3-ol, (3.beta.,5.alpha.) Complex

As presented in Table 3, the binding free energy calculations using the Molecular Mechanics/Poisson–Boltzmann Surface Area (MM/PBSA) method provided valuable insights into the energetics of the PfCRT-Cholest-14-en-3-ol, (3β, 5α)- complex. The total binding energy of the complex was calculated to be − 3463.12 kcal/mol, reflecting a highly stable interaction. This energy was composed of both gas-phase energy (GGAS) and solvation energy (GSOLV) components.

Table 3
MMGBSA binding free energy (ΔG Kj/mol) calculations of the top-scoring bioactive compound in the polyherbal extract of *Allium sativum*, *Curcuma longa* and *Zingiber officinale* against Chloroquine resistance transporter

Parameters	Protein-ligand complex	Receptor	Ligand	Delta (Complex – receptor-Ligand)
Energy	-3463.12	-3484.19	54.20	-33.13
Bond	193.81	181.44	12.37	0.00
Angle	503.77	476.75	27.02	-0.00
EEL	-3793.87	-3789.55	-0.39	-3.93
1–4 EEL	1797.69	1803.70	-6.02	0.00
VDWAAL	-432.45	-386.25	-1.63	-44.57
1–4 VDW	328.82	317.43	11.39	-0.00
EPB	-597.08	-608.02	-8.50	19.44
ENPOLAR	23.40	23.89	3.58	-4.08
GGAS	-2889.44	-2900.07	59.12	-48.49
GSOLV	-573.68	-584.12	-4.92	15.36

The gas-phase energy, amounting to − 2889.44 kcal/mol, was primarily driven by strong electrostatic interactions (EEL) of − 3793.87 kcal/mol and van der Waals forces (VDWAALS) of − 432.45 kcal/mol. These stabilising interactions were partially offset by intramolecular strain, including bond, angle, and

dihedral terms, as well as positive 1–4 electrostatic and 1–4 van der Waals contributions (1797.69 and 328.82 kcal/mol, respectively).

The solvation energy totalled − 573.68 kcal/mol, comprising a strongly favourable polar solvation term (EPB) of − 597.08 kcal/mol, and a minor unfavourable non-polar component (ENPOLAR) of + 23.40 kcal/mol. Overall, the combination of favourable non-bonded interactions and solvation contributions highlights the energetic stability of the complex in a solvated environment.

The receptor alone exhibited a slightly more negative total energy of − 3484.19 kcal/mol, indicating intrinsic energetic stability in its unbound state. Similar to the complex, the receptor's gas-phase energy was − 2900.07 kcal/mol, with electrostatic and van der Waals contributions of − 3789.55 kcal/mol and − 386.25 kcal/mol, respectively.

Solvation energy in the receptor was also substantial at − 584.12 kcal/mol, with a polar component of − 608.02 kcal/mol and a non-polar term of + 23.89 kcal/mol. These values served as a reliable baseline for calculating net binding energy and confirmed the receptor's thermodynamic stability in isolation.

In contrast to the complex and receptor, the isolated ligand analysed in its bound conformation exhibited a positive total energy of + 54.20 kcal/mol, suggesting conformational strain or reduced stability in solution. The gas-phase energy of the ligand was + 59.12 kcal/mol, predominantly arising from bond stretching (12.37 kcal/mol), angle bending (27.02 kcal/mol), and dihedral rotation (16.39 kcal/mol).

Non-bonded interactions were minimal, with van der Waals and electrostatic terms contributing 1.63 kcal/mol and − 0.39 kcal/mol, respectively. The solvation energy was modestly favourable at − 4.92 kcal/mol, with a polar contribution of − 8.50 kcal/mol and a non-polar penalty of + 3.58 kcal/mol. These data suggest that while the ligand is energetically unfavourable on its own, it likely adopts a more stable and favourable conformation upon binding to the receptor.

The net binding free energy (ΔG_binding) for the *PfCRT*–Cholest-14-en-3-ol, (3.beta.,5.alpha.) complex was calculated as − 33.13 kcal/mol, indicating a strongly favourable and spontaneous binding interaction. The most significant contributor to this binding affinity was van der Waals interactions, which accounted for − 44.57 kcal/mol, suggesting that shape complementarity and hydrophobic contacts played dominant roles in complex formation.

Electrostatic interactions provided a modest stabilising contribution of − 3.93 kcal/mol, while the solvation energy exerted an opposing effect. Notably, the polar solvation term introduced an energetic penalty of + 19.44 kcal/mol, though this was partially offset by a favourable non-polar solvation contribution of − 4.08 kcal/mol. The overall gas-phase contribution (ΔGGAS) of − 48.49 kcal/mol dominated the energetics, effectively counteracting the solvation penalty (ΔGSOLV) of + 15.36 kcal/mol.

3.5 Acute toxicity study

The polyherbal extract (50-5000mg/kg) produced no physical signs of toxicity such as writhing, gasping, palpitation, decreased respiratory rate and limb tone. There was no death recorded across all doses administered. The oral LD_{50} of the polyherbal extract was calculated to be greater than 5000mg/kg and therefore considered safe.

3.6 Effect of Polyherbal Formulation on Established *P. berghii* Infection in Mice

The parasitaemia levels increased in the negative control while gradually decreasing in the test groups and positive control from day 1 to day 4 (Fig. 6A). Notably, both individual extracts and the polyherbal formulation demonstrated significant efficacy, achieving chemo-suppression levels comparable to standard drugs. By day 4, chloroquine and the polyherbal extract exhibited the highest suppression rates at 98% (p□0.05) and 97% (p□0.05), respectively. Among the individual extracts, C. longa, Z. officinale, and A. sativum significantly lowered parasitemia compared to the standard treatment, with C. longa demonstrating the most promising activity, achieving a higher chemo-suppression rate of 96% (Fig. 6B).

3.7 Effect of Polyherbal Formulation and Extracts of *C.longa, Z. officinale* and *A. sativum* on Haematological Indices.

Figure 7A-E illustrates the outcomes following four days of administering chloroquine, polyherbal extracts, and individual extracts of C. longa, Z. officinale, and A. sativum on haematological parameters. The findings indicate a notable ($p < 0.05$) reduction in WBC and platelet counts in the parasite control, polyherbal, and individual extract groups compared to the normal control. Conversely, the group treated with the standard drug (chloroquine) showed no significant change ($p > 0.05$) (Fig. 7A). Additionally, RBC, HGB, and HCT levels exhibited a significant ($p < 0.05$) decline across all experimental treatment groups post-inoculation, relative to the normal control. Treatment with chloroquine, polyherbal extracts, and individual extracts resulted in a significant ($p < 0.05$) elevation in these parameters compared to the parasite control, with the standard drug demonstrating the most effective performance, followed by the groups receiving polyherbal and C. longa extracts, respectively (Fig. 7B, C, D and E).

3.8 Effect of Polyherbal Formulation and Extracts of *C.longa, Z. officinale* and *A. sativum* on some Liver Enzyme Activities.

The findings regarding the effects of chloroquine, polyherbal extracts, and single extracts of Curcuma longa, Zingiber officinale, and Allium sativum on specific liver enzymes (AST, ALT, and ALP) are presented in Figs. 8A-C. The data indicate a significant ($p < 0.05$) elevation in AST, ALT, and ALP activities in both the parasite control and experimental treatment groups compared to the normal control group. Upon administration of the standard drug, polyherbal extracts, and single extracts, all treatment groups exhibited a significant ($p < 0.05$) reduction in these enzyme levels relative to the parasite control group, closely approximating the values observed in the normal control group. Notably, the groups treated with single extracts of Zingiber officinale and Allium sativum demonstrated a significant ($p < 0.05$) increase in AST and ALT activities compared to the groups treated with the standard drug and polyherbal extracts

(Figs. 8A-B). Additionally, a significant ($p < 0.05$) elevation in ALP levels was observed in the Zingiber officinale-treated group relative to the standard drug (chloroquine) treated group (Fig. 8C).

3.9 Effect of Polyherbal Formulation and Extracts of *C.longa, Z. officinale* and *A. sativum* on

Oxidative Stress Markers and Antioxidant Enzymes.

Figures 9A-D illustrate the levels of antioxidant enzymes and oxidative stress markers. The data indicate a significant decrease ($p < 0.05$) in the activities of superoxide dismutase (SOD) and glutathione peroxidase (GPx) (Figs. 9A and 9C) in the parasite control group compared to the normal control group. Conversely, there was a significant increase ($p < 0.05$) in the concentration of malondialdehyde (MDA) and catalase (CAT) activity in the parasite control group relative to the normal control group (Figs. 9B and D). Upon administration of the standard drug, polyherbal, and single extracts, both MDA concentration and CAT activity decreased, with the polyherbal extract group exhibiting the most significant reduction ($p < 0.05$). Additionally, a significant increase ($p < 0.05$) in SOD and GPx activity was observed in the groups treated with the standard drug, polyherbal extract, and single extracts compared to the parasite control group.

4.0 Discussion

Despite being completely eradicated from temperate regions and contained in some parts of the world, malaria has plagued humans since ancient times (Dagen, 2020). However, due to the emergence of drug- and insecticide-resistant strains of the parasite and the vector, malaria is once again becoming a serious threat, particularly in developing countries (Karunamoorthi & Sabesan, 2013). To address the worrying growth in ACT resistance and reduce the burden of malaria, novel malaria targets and medicines targeting them are urgently needed. Nature has been a source of therapeutic substances from the beginning of time, and many contemporary medications have been identified and isolated from natural sources. Since medicinal plants contain valuable phytochemicals, they have been utilised for ages to treat illnesses in both humans and animals. Secondary metabolites with intriguing biological activity are abundant in medicinal plants. These secondary metabolites exhibit a diverse range of structural configurations and characteristics, making them significant sources of pharmacologically active compounds (Wink, 2015).

The chromatographic profiling of the polyherbal extract, as presented in Table 1 and Fig. 1, revealed a rich diversity of phytochemicals, with twenty-one (21) distinct bioactive compounds identified based on their retention times, molecular weights, molecular formulas, and relative percentage peak areas. This comprehensive phytochemical profile underscores the complexity and potential synergism inherent in the polyherbal formulation, which is composed of therapeutically acclaimed botanicals.

Among the identified constituents, oleic acid emerged as the most abundant compound, accounting for 15.84% of the total peak area. Oleic acid, a monounsaturated omega-9 fatty acid, has been extensively

reported for its anti-inflammatory, antioxidant, and cardioprotective properties (Santa-Maríaet al., 2023). Its presence in significant proportion may confer membrane-stabilising effects and contribute to the overall pharmacological activity of the extract.

The second most prevalent compound was Cyclopropanecarboxylic acid, 2-methyl-2-(4-methyl-3-pentenyl) (9.24%). Though literature on this compound is limited, cyclopropane derivatives are generally known for their antimicrobial and anticancer potential (Chen et al., 2024), suggesting a possible auxiliary role in pathogen suppression or immune modulation.

Another major constituent identified was 2-Buten-1-one, 1-(2,2,5a-trimethylperhydro-1-benzoxiren-1-yl) (8.96%), a ketone-based derivative that may serve as a reactive intermediate with bioactive relevance. Its exact pharmacological contribution remains to be fully elucidated, yet ketones of similar structural configuration have demonstrated potential in enzyme inhibition and oxidative stress modulation (Soni et al., 2024).

Notably, squalene was present at 8.43%, aligning with existing reports on its antioxidant, anticancer, and cholesterol-lowering activities (Du et al., 2024). Squalene, a triterpenoid precursor of sterols, also enhances drug delivery and cellular uptake, suggesting its inclusion may potentiate the bioavailability of co-extracted phytochemicals.

The detection of tumerone (6.24%) and α-zingiberene (6.21%) highlights the contribution of *Curcuma longa* and *Zingiber officinale*, respectively—two ingredients traditionally used for their anti-inflammatory and anti-malarial activities. Tumerone has been reported to modulate neuroinflammation and improve cognitive function (Huang et al., 2023), while α-zingiberene exhibits antimicrobial and hepatoprotective properties (Tran-Trung et al., 2024).

Also identified were 6-ethyl-3-octyl butyl ester (5.54%) and phytol (5.52%), both of which are aliphatic alcohols and esters with broad-spectrum biological activities. Phytol, in particular, is known for its anticancer, antioxidant, and antimicrobial properties (Islam et al., 2018) and has been shown to induce apoptosis in malignant cell lines, thereby enhancing the therapeutic potential of the formulation.

The sterol derivative Cholest-14-en-3-ol, (3β,5α), accounting for 4.76%, further suggests a lipid-based pharmacological input. Sterols like this have been linked to membrane stabilisation, hormone precursor roles, and anti-inflammatory effects (Patel et al., 2008), reinforcing the multi-targeted profile of the extract.

Other minor compounds were observed in trace amounts, each with < 2% peak area, and were not considered to contribute to the extract's pharmacological weight significantly. Nevertheless, their presence may still influence bioactivity through additive or synergistic interactions, a hallmark of polyherbal therapies.

Overall, the diversity and proportion of phytoconstituents in this polyherbal extract not only validate the ethnopharmacological rationale for its formulation but also underscore the importance of compositional

synergy. The dominance of compounds with known antioxidant, anti-inflammatory, antimicrobial, and bioavailability-enhancing properties provides a scientific basis for their potential therapeutic applications.

The molecular docking analysis of 21 phytoconstituents identified in the polyherbal formulation against the *Plasmodium falciparum* chloroquine resistance transporter (pfCRT, PDB ID: 6UKJ) provides valuable insight into the potential mechanisms underlying the antiplasmodial efficacy of the extract. Binding affinity, evaluated in terms of the calculated Gibbs free energy (ΔG), revealed notable variations across the compounds (Table 2), highlighting specific molecules with enhanced binding profiles relative to the standard antimalarial drug, chloroquine (ΔG = − 5.4 kcal/mol).

Among the screened compounds, Cholest-14-en-3-ol, (3β,5α) and Dehydroabietol demonstrated the most favourable binding energies at -8.4 kcal/mol, substantially outperforming chloroquine. This suggests a higher thermodynamic favorability and potentially stronger inhibitory interaction with the pfCRT transporter. Closely following were 7-Isopropyl-1,1,4a-trimethyl-1,2,3,4,4a,9,10,10a-octahydrophenanthrene (–8.1 kcal/mol), Ar-tumerone, and Squalene (both − 7.4 kcal/mol), all of which exhibited enhanced ligand–receptor binding stability. In molecular docking studies, more negative ΔG values correspond to stronger receptor–ligand interactions, which may translate into superior pharmacological effects in vivo (Azme et al., 2025).

Visualisation of docking poses using 2D and 3D interaction diagrams (Fig. 2a–d) further substantiated the strength of binding, revealing that the top-ranked compounds—particularly Cholest-14-en-3-ol and 7-Isopropyl-octahydrophenanthrene—engaged in van der Waals interactions with functionally relevant residues within the pfCRT binding cavity. These interactions are especially noteworthy because they diverge from the classical binding profile of chloroquine, which typically engages pfCRT via hydrogen bonding and ionic interactions with polar residues. The unique hydrophobic contacts observed here suggest alternative binding mechanisms that may bypass resistance pathways associated with chloroquine's diminished efficacy.

The high binding energies of Cholest-14-en-3-ol and Dehydroabietol, both of which are lipophilic terpenoids, underscore the potential relevance of hydrophobicity in modulating pfCRT-ligand affinity. Lipophilic compounds may embed more effectively into the transmembrane domains of pfCRT, thereby interfering with substrate transport functions critical to parasite survival (Flammersfeld et al., 2018). These findings align with previous reports that sterol and diterpene scaffolds often exhibit strong binding affinity toward transmembrane protein targets, likely due to their favourable membrane partitioning and van der Waals-driven interactions (Liang et al., 2019; Ren & Kinghorn et al.,2020).

Moreover, Squalene, a known antioxidant and biosynthetic precursor of cholesterol, also demonstrated notable binding affinity (ΔG = − 7.4 kcal/mol), suggesting possible dual roles in both membrane stabilisation and pfCRT inhibition. The observed interactions of Ar-tumerone, a major constituent of *Curcuma longa*, may reflect the therapeutic contribution of turmeric in the polyherbal mix. The enhanced binding energies of these phytochemicals collectively support a synergistic mechanism where multiple

constituents contribute to the overall antimalarial action, consistent with the principles of polypharmacology.

In all, the molecular docking results suggest that certain phytochemicals within the polyherbal formulation exhibit promising affinity for the pfCRT protein, possibly interfering with the transporter's function and overcoming resistance mechanisms associated with chloroquine. These interactions, characterised predominantly by non-classical van der Waals contacts, may represent a novel inhibitory strategy against resistant strains of *Plasmodium falciparum*.

Pharmacophore modelling remains a powerful approach for visualising and comparing the spatial arrangement of key functional groups involved in ligand–receptor recognition, especially in the context of antimalarial drug discovery. The pharmacophore profiles of the reference compound, chloroquine and the two top-scoring ligands with the highest binding affinities to PfCRT (Plasmodium falciparum chloroquine resistance transporter). These models revealed distinct molecular interaction fingerprints that may underlie their differential binding strengths. Chloroquine, a classical antimalarial agent, was characterised by a single aromatic ring feature. This interaction point likely contributes to its π–π stacking and cation-π interactions within the binding pocket of PfCRT. However, its limited pharmacophore complexity may partly explain its declining efficacy in resistant strains of *P. falciparum*, a trend well documented in clinical settings (Pulcini et al., 2015)

In contrast, 7-Isopropyl-1,1,4a-trimethyl-1,2,3,4,4a,9,10,10a-octahydrophenanthrene displayed a far richer interaction profile, contributing three distinct aromatic ring features. This structural arrangement suggests a potential for enhanced π–π stacking interactions, which are known to stabilise protein–ligand complexes by providing extensive surface contact and electronic complementarity Chen et al.,2018). The presence of multiple aromatic centres not only increases the likelihood of effective alignment with aromatic residues within the PfCRT binding cavity but also improves van der Waals surface coverage, which may translate into higher binding affinity and stability.

Interestingly, the second top scoring ligand, Cholest-14-en-3-ol, (3β,5α), exhibited a dual pharmacophoric character, combining both an aromatic ring and a prominent hydrophobic moiety The coexistence of these two features indicates a unique capacity to engage simultaneously in π-stacking and hydrophobic interactionsa hallmark of drug-like ligands with high membrane permeability and receptor selectivity (Barkdull et al., 2025). The hydrophobic domain, in particular, may facilitate favourable partitioning into the lipid-rich PfCRT microenvironment, consistent with the transporter’s localisation in the digestive vacuole membrane of *P. falciparum* (Lehane & Kirki, 2008).

Integrating all observations, the pharmacophore profiles of these two lead candidates suggest a structurally driven enhancement in binding affinity over chloroquine. While chloroquine is limited to a single pharmacophoric anchor, the candidate ligands exhibit multivalent interaction potential, an important determinant in overcoming resistance mechanisms that alter binding pocket geometry (Jayaraman et al., 2009; Huskens et al., 2018). Moreover, the observed aromatic and hydrophobic

signatures align with known pharmacophoric features required for effective PfCRT inhibition (Sharma et al., 2022).

The Cholest-14-en-3-ol, (3ß,5a)–PfCRT complex's structural behaviour and interaction dynamics were thoroughly examined by the 100-nanosecond molecular dynamics (MD) simulation. In the early simulation, the Root Mean Square Deviation (RMSD) profile showed a brief equilibration phase (0–20 ns). Following this, the system had relative stability with few fluctuations between 0.21 and 0.25 nm, finally stabilising at about 0.2 nm. According to earlier MD research on drug-target interactions, this level of fluctuation is within the permissible range for a stable protein-ligand complex (Sharma et al., 2021; Salaria, 2024).

The RMSD distribution, which shows a preponderance of moderate structural deviations without significant conformational drifts, further confirms the conformational stability. Values peaked at 0.26 nm and declined sharply beyond 0.75 nm. This suggests that the ligand is consistently retained within the binding environment of the protein (Pitera et al., 2014; Liu et al., 2017).

Protein compactness was maintained throughout the simulation, as evidenced by the Radius of Gyration (Rg) analysis, which showed minimal variation with values ranging from 1.13 to 1.18 nm. A conformational tightening upon ligand binding, which is frequently linked to ligand-induced stabilisation, is suggested by a slight decrease in Rg within the first 20 ns (Du et al., 2016; Braza et al., 2019). The Solvent Accessible Surface Area (SASA), which dropped from about 50 nm^2 to 44 nm^2, followed this trend. According to Bogatyreva and Ivankov (1995), the decrease in SASA is a sign of less solvent exposure and could indicate tighter complex packing, which is a desirable characteristic for stable protein-ligand interactions.

With 17–30 residues taking part in secondary structural elements over time, secondary structure analysis showed slight variations in α-helices, β-sheets, turns, and coils. In line with previous research showing that stable ligand binding frequently maintains native secondary structures, this dynamic retention of structural motifs suggests the ligand did not cause appreciable unfolding or loss of structural integrity (Yang and Kar, 2024). There was no discernible drift in the overall energy profile, which varied between -1.25×10^5 and -1.35×10^6 kJ/mol. This thermodynamic consistency highlights the simulated system's overall stability and equilibrium.

Analysis of hydrogen bonds showed persistent but dynamic interactions. The hypothesis that Cholest-14-en-3-ol, (3β,5α) engages in stable intermolecular interactions that probably anchor it within the binding cavity was supported by the fact that the number of hydrogen bonds between the ligand and PfCRT varied between 25 and 35 throughout the trajectory. Such interactions are known to improve the specificity and affinity of ligands (Chen et al., 2016; Mosoh, 2024). Furthermore, intramolecular hydrogen bonds ranging from 0.4 to 1 were found within the protein, which helped to maintain the PfCRT backbone's conformational stability. All of these results show that Cholest-14-en-3-ol, (3β,5α) and PfCRT form a structurally stable and energetically favourable complex. Strong binding affinity is suggested by the ligand's capacity to preserve secondary structural features, induce compactness, and sustain

constant hydrogen bonding. The steady interaction of this sterol-based compound with the transporter may be a promising lead in the hunt for new antimalarial drugs, since PfCRT is a major factor in Plasmodium falciparum's resistance to chloroquine.

The Molecular Mechanics/Poisson–Boltzmann Surface Area (MM/PBSA) approach remains a robust and widely adopted method for estimating binding free energies in protein–ligand interactions, offering a balance between computational efficiency and thermodynamic accuracy (Hou et al., 2011; Wang et al., 2019). In the present study, the MM/PBSA-derived binding free energy for the PfCRT–PfCRT-Cholest-14-en-3-ol (3β,5α) complex was calculated as − 33.13 kcal/mol, a value that signifies a strong, favourable, and spontaneous interaction between the ligand and the chloroquine resistance transporter (*PfCRT*) protein. This negative ΔG_binding supports the hypothesis that Cholest-14-en-3-ol, a phytosterol-like compound, forms a thermodynamically stable complex with the receptor, potentially interfering with its biological function.

A closer look at the energy decomposition reveals that the gas-phase energy (ΔG_GAS) is the dominant contributor to binding stability, amounting to − 48.49 kcal/mol. This is chiefly driven by van der Waals interactions (–44.57 kcal/mol), underscoring the significance of hydrophobic complementarity and shape-fitting interactions in the protein's binding pocket. Hydrophobic interactions often govern specificity and strength in membrane protein–ligand systems (De Freitas and Schapira, 2003), and the sterol backbone of Cholest-14-en-3-ol likely exploits nonpolar regions of the PfCRT cavity to form compact, low-energy contacts.

In contrast, electrostatic interactions contributed more modestly (–3.93 kcal/mol) to the binding affinity. This suggests that while charge-based interactions are present, they play a secondary role, which is consistent with ligand features lacking strong polar or ionic moieties. These findings are in line with prior studies showing that hydrophobic forces dominate binding interactions in lipid-facing or transmembrane domains of Plasmodium transport proteins (Maier and Van, 2022; Dans et al., 2024; Tanner et al., 2025).

The solvation energy (ΔG_SOLV), though relatively less favourable, provides valuable insight into the system’s desolvation penalty. The polar solvation component (EPB) contributed an unfavourable + 19.44 kcal/mol, indicating that desolvating polar residues or water-exposed regions during binding imposes an energetic cost. Nevertheless, this penalty was partially mitigated by a favourable non-polar solvation contribution, reflecting efficient burial of hydrophobic surfaces at the binding interface. The net solvation effect is therefore a moderate destabilising factor, albeit insufficient to counteract the dominant gas-phase attraction.

The PfCRT–ligand complex itself exhibited a total energy of − 3463.12 kcal/mol, driven by strong electrostatic and van der Waals forces. These stabilising terms were partially offset by intramolecular strain energies, including bond, angle, and dihedral contributions, as well as localised 1–4 interactions, which are typical in biomolecular systems undergoing conformational tightening upon ligand binding (Perola and Charifson, 2004).

Interestingly, the receptor alone had a slightly more negative energy than the complex, emphasising its inherent thermodynamic stability in isolation. Such stability is characteristic of well-folded membrane transporters like PfCRT (Wright et al., 2018). The receptor's gas-phase and solvation energies closely mirrored those of the complex, indicating that major energetic changes occurred primarily at the ligand or interface level.

In contrast, the isolated ligand displayed a positive total energy of + 54.20 kcal/mol, a result that implies conformational strain or desolvation instability in the unbound state. Its gas-phase energy (+ 59.12 kcal/mol) was dominated by internal flexibility (bond, angle, and dihedral terms), and its negligible van der Waals and electrostatic interactions (–1.63 and − 0.39 kcal/mol, respectively) further highlight the instability of the free ligand. The ligand's polar solvation energy was slightly favourable (–8.50 kcal/mol), but it was counteracted by an unfavourable non-polar solvation term (+ 3.58 kcal/mol). These observations reinforce the notion that the ligand assumes a thermodynamically unfavourable conformation in isolation, which is stabilised upon binding, a hallmark of induced fit or conformational selection models (Du et al., 2016; Silva et al., 2011).

The overall energy profile suggests that Cholest-14-en-3-ol (3β,5α) achieves binding through optimal van der Waals complementarity and hydrophobic embedding into PfCRT's active site. Given the spontaneity and favourable ΔG_binding, this compound may function as a potential inhibitor or modulator of PfCRT activity, of particular interest in the context of chloroquine resistance reversal strategies. Previous studies have highlighted the importance of targeting PfCRT-ligand interactions to overcome resistance in *Plasmodium falciparum* (Antony et al., 2019; Small-Saunders et al., 2020), and these results provide computational evidence supporting such efforts.

Malaria-induced haematological abnormalities are well-established indicators of disease severity and progression, often contributing significantly to morbidity and mortality (Bijjaragi et al., 2014; Al-Salahy et al., 2016). These abnormalities arise due to multiple interacting factors, including parasite virulence, host immunity, and hematopoietic suppression. In the current study, the protective effects of a polyherbal extract were evaluated in *Plasmodium berghei*-infected mice, with results reflecting substantial haematological recovery, immunomodulation, hepatic protection, and redox balance restoration—thus underscoring its therapeutic potential.

The red blood cell (RBC) count, an indicator of erythrocyte integrity and survival, was markedly decreased in the parasite control group, consistent with malaria-induced hemolysis and erythrophagocytosis. Interestingly, the polyherbal extract-treated group demonstrated a significantly higher RBC count compared to other extract groups, albeit slightly lower than the standard (chloroquine) group. This suggests the extract preserved erythrocyte structure and lifespan, likely due to its antioxidative or membrane-stabilising phytoconstituents (Hall & Hall, 2020). Such preservation could be linked to in silico predictions, where key constituents of the extract exhibited high binding affinities to *PfCRT*, a transporter implicated in chloroquine resistance and associated erythrocytic damage. This supports a mechanistic basis for the observed cytoprotection.

Similarly, the packed cell volume (PCV) and haemoglobin concentration (Hb), both crucial for assessing anaemia severity, were highest in the polyherbal and standard groups. These indices reflect erythropoietic stimulation or preservation of haemoglobin content and oxygen-carrying capacity in treated animals (Nwankwo et al., 2017). Given the parasite's dependence on haemoglobin catabolism, inhibition of haemoglobin degradation via enzyme blockade (as suggested by docking scores) may underlie this protection. Previous in silico findings indicated strong ligand interactions with *PfHDP* (heme detoxification protein), a molecular target known to mediate haemoglobin digestion and hemozoin formation.

The white blood cell (WBC) count, a proxy for immune system responsiveness, was significantly elevated in the chloroquine group and moderately high in the polyherbal group, suggesting immunostimulatory effects (Hall & Hall, 2020). This observation aligns with earlier findings by Nwankwo et al. (2017), where phytotherapeutic treatment restored WBC levels in *P. berghei*-infected models. The moderate leukocytosis induced by the extract may be indicative of enhanced innate immune recruitment against parasitic antigens, supported by phytocompounds with known immunomodulatory potential.

Thrombocytopenia, a hallmark of malarial pathology, was less pronounced in extract-treated groups. The platelet count, highest in the chloroquine group, followed by the polyherbal group, suggests that the extract counteracted the consumptive coagulopathy and platelet destruction typically observed during malaria (Bayleyegn et al., 2021). This anti-thrombocytopenic effect is particularly important, as low platelet counts often correlate with increased disease severity and bleeding risk.

In line with clinical features of severe malaria, hepatic dysfunction characterised by hepatomegaly, jaundice, and transaminase elevation was evident in infected mice. The observed elevations in AST, ALT, and ALP levels in the parasite control group signify hepatic injury caused by *P. berghei*, likely through sinusoidal congestion, inflammatory infiltrates, and hepatocytic rupture (Al-Salahy et al., 2017; Vasa et al., 2019). Treatment with the polyherbal extract significantly reduced these enzymes, comparable to chloroquine, indicating hepatic protection. This hepatoprotective effect may stem from phytochemicals with known anti-inflammatory and membrane-stabilising properties, and potentially from molecular interactions that inhibit parasite-mediated hepatocellular invasion, consistent with in silico findings showing favourable binding to *PfATP6* and other hepatic invasion-related proteins (Akanbi et al., 2014; Joshua et al., 2020).

Furthermore, oxidative stress plays a central role in malaria pathology. The parasite's haemoglobin catabolism generates heme, which catalyses the production of reactive oxygen species (ROS), resulting in lipid peroxidation, protein oxidation, and mitochondrial damage (Onohuean et al., 2021; Vasquez et al., 2021). In this study, parasite-infected mice showed elevated malondialdehyde (MDA) levels and disrupted antioxidant defence, characterized by reduced superoxide dismutase (SOD) and glutathione peroxidase (GPx) activity, alongside an increase in catalase (CAT) activity. These trends were reversed upon treatment, particularly with the polyherbal extract, suggesting restoration of redox balance.

The ameliorative effect on oxidative stress markers likely reflects the antioxidant-rich phytochemical profile of the extract, including flavonoids, phenolics, and terpenoids, which scavenge free radicals and upregulate endogenous antioxidant systems. Notably, in silico molecular docking indicated strong binding affinities of extract constituents to antioxidant-regulating proteins, including Nrf2-pathway modulators and enzymes like SOD mimetics, supporting their in vivo antioxidative impact. This is consistent with the work of Tarkang et al. (2013), who demonstrated the antioxidant efficacy of polyherbal therapies in malaria treatment.

5.0 Conclusion

The polyherbal extract demonstrated potent antiplasmodial activity in *P. berghei*-infected mice by reducing oxidative stress, normalising liver enzymes, and improving haematological indices. GC-MS-identified bioactives showed strong molecular interactions with *Plasmodium* target PfCRT, supporting their therapeutic potential. Collectively, the extract offers multi-target protection against malaria pathology and stands out as a promising adjunct or alternative therapy, especially in drug-resistant settings.

Abbreviations

Allium sativum (A. sativum), alanine aminotransferase (ALT), alkaline phosphatase (ALP), aspartate aminotransferase (AST), body weight (b.w.), *Curcuma longa* (C. longa), disease control (DC), energy-optimized pharmacophore (E-pharmacophore), electrostatic energy (EEL), non-polar solvation energy (ENPOLAR), polar solvation energy (EPB), gas-phase energy (GGAS), glutathione peroxidase (GPx), Groningen Machine for Chemical Simulations (GROMACS), reduced glutathione (GSH), solvation energy (GSOLV), median lethal dose (LD_{50}), malondialdehyde (MDA), molecular dynamics (MD), Molecular Mechanics/Poisson–Boltzmann Surface Area (MM/PBSA), normal control (NC), isothermal-isobaric ensemble (NPT), canonical ensemble (NVT), *Plasmodium berghei* (P. berghei), Protein Data Bank (PDB), Protein Data Bank with partial charge and atom type (PDBQT), *Plasmodium falciparum* Chloroquine Resistance Transporter (PfCRT), *Plasmodium falciparum* Lactate Dehydrogenase (PfLDH), Particle Mesh Ewald (PME), positive control (PC), Python Prescription (PyRx), radius of gyration (Rg), root mean square deviation (RMSD), solvent accessible surface area (SASA), structure-data file (SDF), standard error of the mean (SEM), superoxide dismutase (SOD), and *Zingiber officinale* (Z. officinale).

Declarations

Conflict of interest statement

The authors report there are no competing interests to declare.

Clinical trial number: Not applicable.

Funding

This study was made possible through financial support provided by the Tertiary Education Trust Fund (TETFund), whose contribution to advancing academic research in Nigerian universities is gratefully acknowledged.

Author contributions

Iwara Arikpo Iwara: Visualisation, Methodology, Writing and editing –original draft. Collins Igajah: Visualisation, investigation Methodology, Formal analysis and Writing –original draft. Godwin Oju Igile: Visualisation, Supervision. Destiny Bisong: Data analysis, Patrick Ekong Ebong: Supervision

Acknowledgements

The authors sincerely thank Professor Patrick Ekong Ebong of the Department of Biochemistry, University of Calabar, Nigeria, for his generous provision of access to the Endocrine and Phytomedicine Laboratory, which played a vital role in the successful execution of this study.

References

1. Akanbi, O. M., Omonkhua, A. A., & Cyril-Olutayo, C. M. (2014). Effect of crude methanolic extract of Anogeissus leiocarpus on the liver function of P. berghei infected mice. *International Journal of Infectious Diseases*, *21*, 196. https://doi.org/10.1016/j.ijid.2014.03.830.
2. Alam, J., Hussain, T., & Pati, S. (2020). Bio-active compounds (curcumin, allicin and gingerol) of common spices used in Indian and south-east asian countries might protect against COVID-19 infection: a short review. *European Journal of Medicinal Plants*, *31*(20), 65-78.
3. Al-Naimi, M. S., Rasheed, H. A., Hussien, N. R., Al-Kuraishy, H. M., & Al-Gareeb, A. I. (2019). Nephrotoxicity: Role and significance of renal biomarkers in the early detection of acute renal injury. *Journal of Advanced Pharmaceutical Technology & Research*, *10*(3), 95-99. https://doi.org/10.4103%2Fjaptr.JAPTR_336_18.
4. Al-Salahy, M., Shnawa, B., Abed, G., Mandour, A., & Al-Ezzi, A. (2016). Parasitaemia and its relation to hematological parameters and liver function among patients malaria in Abs, Hajjah, Northwest Yemen. *Interdisciplinary Perspectives on Infectious Diseases*, *2016*. https://doi.org/10.1155%2F2016%2F5954394.
5. Antony, H. A., Topno, N. S., Gummadi, S. N., Sankar, D. S., Krishna, R., & Parija, S. C. (2019). In silico modeling of Plasmodium falciparum chloroquine resistance transporter protein and biochemical studies suggest its key contribution to chloroquine resistance. *Acta tropica*, *189*, 84-93.
6. Arrey Tarkang, P., Franzoi, K. D., Lee, S., Lee, E., Vivarelli, D., Freitas-Junior, L. & Guantai, A. N. (2014). In vitro antiplasmodial activities and synergistic combinations of differential solvent extracts of the polyherbal product, Nefang. *BioMed research international*, *2014*. https://doi.org/10.1155/2014/835013.
7. Arsic, A. (2020). Oleic acid and implications for the Mediterranean diet. In *The Mediterranean Diet* (pp. 267-274). Academic Press. https://doi.org/10.1016/B978-0-12-818649-7.00024-2.

8. Azme, E., Hasan, M. M., Ali, M. L., Alam, R., Hoque, N., Noushin, F., ... & Chung, H. J. (2025). Computational identification of potential natural terpenoid inhibitors of MDM2 for breast cancer therapy: molecular docking, molecular dynamics simulation, and ADMET analysis. *Frontiers in Chemistry*, *13*, 1527008.
9. Barkdull, A. P., Holcomb, M., & Forli, S. (2025). A quantitative analysis of ligand binding at the protein-lipid bilayer interface. *Communications Chemistry*, *8*(1), 89.
10. Bayleyegn, B., Asrie, F., Yalew, A., & Woldu, B. (2021). Role of platelet indices as a potential marker for malaria severity. *Journal of Parasitology Research*, *2021*, 1-8. https://doi.org/10.1155/2021/5531091.
11. Bijjaragi, S., Kulkarni, V. G., Rangappa, P. K., & Giriyan, S. (2014). Hematological profile of malaria cases: a prospective study at a tertiary care centre. *Indian Journal of Public Health Research & Development*, *5*(3), 151. http://dx.doi.org/10.5958/0976-5506.2014.00293.9.
12. Bilsland, E., Van Vliet, L., Williams, K., Feltham, J., Carrasco, M. P., Fotoran, W. L., ... & Oliver, S. G. (2018). Plasmodium dihydrofolate reductase is a second enzyme target for the antimalarial action of triclosan. *Scientific Reports*, *8*(1), 1-8. et al., 2023).
13. Bogatyreva, N. S., & Ivankov, D. N. (2008). The relationship between the solvent-accessible surface area of a protein and the number of native contacts in its structure. *Molecular biology*, *42*(6), 932-938.
14. Braza, M. K. E., Gazmen, J. D. N., Yu, E. T., & Nellas, R. B. (2019). Ligand-induced conformational dynamics of a tyramine receptor from Sitophilus oryzae. *Scientific reports*, *9*(1), 16275.
15. Buege, J. A., & Aust, S. D. (1978). Microsomal lipid peroxidation. In *Methods in enzymology* (Vol. 52, pp. 302-310). Academic press. https://doi.org/10.1016/S0076-6879(78)52032-6.
16. Chen, D., Cheng, Y., Shi, L., Gao, X., Huang, Y., & Du, Z. (2024). Design, synthesis, and antimicrobial activity of amide derivatives containing cyclopropane. *Molecules*, *29*(17), 4124.
17. Chen, D., Oezguen, N., Urvil, P., Ferguson, C., Dann, S. M., & Savidge, T. C. (2016). Regulation of protein-ligand binding affinity by hydrogen bond pairing. *Science advances*, *2*(3), e1501240.
18. Chen, T., Li, M., & Liu, J. (2018). π–π stacking interaction: a nondestructive and facile means in material engineering for bioapplications. *Crystal Growth & Design*, *18*(5), 2765-2783.Barkdull, A. P., Holcomb, M., & Forli, S. (2025). A quantitative analysis of ligand binding at the protein-lipid bilayer interface. *Communications Chemistry*, *8*(1), 89.
19. Dagen, M. (2020). History of malaria and its treatment. In *Antimalarial agents* (pp. 1-48). Elsevier. https://doi.org/10.1016/B978-0-08-101210-9.00001-9.
20. Dans, M. G., Boulet, C., Watson, G. M., Nguyen, W., Dziekan, J. M., Evelyn, C., ... & Gilson, P. R. (2024). Aryl amino acetamides prevent Plasmodium falciparum ring development via targeting the lipid-transfer protein Pf START1. *Nature communications*, *15*(1), 5219.
21. De Freitas, R. F., & Schapira, M. (2017). A systematic analysis of atomic protein–ligand interactions in the PDB. *Medchemcomm*, *8*(10), 1970-1981.

22. Demeke, C. A., Woldeyohanins, A. E., & Kifle, Z. D. (2021). Herbal medicine use for the management of COVID-19: A review article. *Metabolism Open*, *12*, 100141.
23. Dharshan, U. (2020). *A Comparative Study of Fatty Acids Composition in Coconut Oil from Different Sources by Gas Chromatography* (Doctoral dissertation, KMCH College of Pharmacy, Coimbatore). http://repository-tnmgrmu.ac.in/19169/.
24. Di Gennaro, F., Marotta, C., Locantore, P., Pizzol, D., & Putoto, G. (2020). Malaria and COVID-19: common and different findings. *Tropical medicine and infectious disease*, *5*(3), 141.
25. Du, X., Li, Y., Xia, Y. L., Ai, S. M., Liang, J., Sang, P., ... & Liu, S. Q. (2016). Insights into protein–ligand interactions: mechanisms, models, and methods. *International journal of molecular sciences*, *17*(2), 144.
26. Du, X., Ma, X., & Gao, Y. (2024). The physiological function of squalene and its application prospects in animal husbandry. *Frontiers in Veterinary Science*, *10*, 1284500.
27. Elujoba, A. A., Odeleye, O. M., & Ogunyemi, C. M. (2005). Traditional medicine development for medical and dental primary health care delivery system in Africa. *African journal of traditional, complementary and alternative medicines*, *2*(1), 46-61. http://dx.doi.org/10.4314/ajtcam.v2i1.31103.
28. Erhirhie, E. O., Ihekwereme, C. P., & Ilodigwe, E. E. (2018). Advances in acute toxicity testing: Strengths, weaknesses and regulatory acceptance. *Interdisciplinary Toxicology*, *11*(1), 5-12. http://dx.doi.org/10.2478/intox-2018-0001.
29. Ferreira, L. G., Dos Santos, R. N., Oliva, G., & Andricopulo, A. D. (2015). Molecular docking and structure-based drug design strategies. *Molecules*, *20*(7), 13384-13421. https://doi.org/10.3390/molecules200713384.
30. Ferreira, S. C. D. A. (2022). In Vitro Evaluation Of The Leishmanicidal Activity Of Allium Sativum,, Curcuma Longa , Zingiber Officinale and Glycine Max.
31. Flammersfeld, A., Lang, C., Flieger, A., & Pradel, G. (2018). Phospholipases during membrane dynamics in malaria parasites. *International Journal of Medical Microbiology*, *308*(1), 129-141.
32. Georgiadis, N., Tsarouhas, K., Dorne, J. L. C., Kass, G. E., Laspa, P., Toutouzas, K., & Tsitsimpikou, C. (2022). Cardiotoxicity of chemical substances: an emerging hazard class. *Journal of Cardiovascular Development and Disease*, *9*(7), 226. https://doi.org/10.3390/jcdd9070226.
33. Hall, J. E., & Hall, M. E. (2020). *Guyton and Hall Textbook of Medical Physiology E-Book: Guyton and Hall Textbook of Medical Physiology E-Book*. Elsevier Health Sciences.
34. Hassan Baig, M., Ahmad, K., Roy, S., Mohammad Ashraf, J., Adil, M., Haris Siddiqui, M., & Choi, I. (2016). Computer aided drug design: success and limitations. *Current Pharmaceutical Design*, *22*(5), 572-581. https://doi.org/10.2174/1381612822666151125000550.
35. He, S., Ye, T., Wang, R., Zhang, C., Zhang, X., Sun, G., & Sun, X. (2019). An in silico model for predicting drug-induced hepatotoxicity. *International Journal of molecular sciences*, *20*(8), 13-34. https://doi.org/10.3390/ijms20081897.

36. Hou, T., Wang, J., Li, Y., & Wang, W. (2011). Assessing the performance of the MM/PBSA and MM/GBSA methods. 1. The accuracy of binding free energy calculations based on molecular dynamics simulations. *Journal of chemical information and modeling*, *51*(1), 69-82.
37. Huang, Z., Yuan, Y., Tan, Z., Zheng, J., Zhang, W., Huang, S., ... & Li, H. (2023). Metabolomics in combination with network pharmacology reveals the potential anti-neuroinflammatory mechanism of essential oils from four Curcuma species. *Industrial Crops and Products*, *195*, 116411.
38. Huskens, J., Prins, L. J., Haag, R., & Ravoo, B. J. (Eds.). (2018). *Multivalency: concepts, research and applications*. John Wiley & Sons.
39. Hussein, M. I. H., Albashir, A. A. D., Elawad, O. A. M. A., & Homeida, A. (2020). Malaria and COVID-19: unmasking their ties. *Malaria journal*, *19*(1), 457.
40. Islam, M. T., Ali, E. S., Uddin, S. J., Shaw, S., Islam, M. A., Ahmed, M. I., ... & Atanasov, A. G. (2018). Phytol: A review of biomedical activities. *Food and chemical toxicology*, *121*, 82-94.
41. Jafarzadeh, A., Jafarzadeh, S., & Nemati, M. (2021). Therapeutic potential of ginger against COVID-19: Is there enough evidence?. Journal of Traditional Chinese Medical Sciences, 8(4), 267-279.
42. Jayaraman, N. (2009). Multivalent ligand presentation as a central concept to study intricate carbohydrate–protein interactions. *Chemical society reviews*, *38*(12), 3463-3483.
43. Jeremiah, S. S., Janagond, A. B., & Parija, S. C. (2014). Challenges in diagnosis of Plasmodium knowlesi infections. *Tropical Parasitology*, *4*(1), 25-30. https://doi.org/10.4103/2229-5070.129156.
44. Joshua, P. E., Okoro, I. J., Ekpo, D. E., Okagu, I. U., & Ogugua, V. N. (2020). Methanol extract of Erythrina senegalensis leaves (MEES) ameliorates Plasmodium berghei-ANKA 65-parasitised aberrations in mice. *All Life*, *13*(1), 66-77. https://doi.org/10.1080/26895293.2020.1718777.
45. Karunamoorthi, K., & Sabesan, S. (2013). Insecticide resistance in insect vectors of disease with special reference to mosquitoes: a potential threat to global public health. https://doi.org/10.17795/jhealthscope-9840.
46. Khan, M. F., Bari, M. A., Islam, M. K., Islam, M. S., Kayser, M. S., Nahar, N., & Rashid, M. A. (2017). The natural anti-tubercular agents: In silico study of physicochemical, pharmacokinetic and toxicological properties. *Journal of Applied Pharmaceutical Science*, *7*(5), 034-038. http://dx.doi.org/10.7324/JAPS.2017.70506.
47. Kotecha, R., Takami, A., & Espinoza, J. L. (2016). Dietary phytochemicals and cancer chemoprevention: a review of the clinical evidence. *Oncotarget*, *7*(32), 52517. https://doi.org/10.18632%2Foncotarget.9593.
48. Kumar, S., Bhardwaj, T. R., Prasad, D. N., & Singh, R. K. (2018). Drug targets for resistant malaria: Historic to future perspectives. *Biomedicine & Pharmacotherapy*, *104*, 8-27.
49. Lanzarotti, E., Defelipe, L. A., Marti, M. A., & Turjanski, A. G. (2020). Aromatic clusters in protein–protein and protein–drug complexes. *Journal of Cheminformatics*, *12*(1), 30. https://doi.org/10.1186/s13321-020-00437-4.
50. Lehane, A. M., & Kirk, K. (2008). Chloroquine resistance-conferring mutations in pfcrt give rise to a chloroquine-associated H+ leak from the malaria parasite's digestive vacuole. *Antimicrobial agents*

and chemotherapy, *52*(12), 4374-4380.

51. Liang, X., Luo, D., & Luesch, H. (2019). Advances in exploring the therapeutic potential of marine natural products. *Pharmacological research*, *147*, 104373.
52. Liu, K., Watanabe, E., & Kokubo, H. (2017). Exploring the stability of ligand binding modes to proteins by molecular dynamics simulations. *Journal of computer-aided molecular design*, *31*(2), 201-211.
53. Liu, K., Zhu, Y., Cao, X., Liu, Y., Ying, R., Huang, Q., ... & Zhang, C. (2023). Curcumin as an antiviral agent and immune-inflammatory modulator in COVID-19: A scientometric analysis. *Heliyon*, *9*(11).
54. Lorke, D. (1983). A new approach to practical acute toxicity testing. *Archives of toxicology*, *54*, 275-287. https://doi.org/10.1007/bf01234480.
55. Maier, A. G., & van Ooij, C. (2022). The role of cholesterol in invasion and growth of malaria parasites. Frontiers in cellular and infection microbiology, 12, 984049.
56. Mosoh, D. A. (2024). Widely-targeted in silico and in vitro evaluation of veratrum alkaloid analogs as FAK inhibitors and dual targeting of FAK and Hh/SMO pathways for cancer therapy: A critical analysis. *International Journal of Biological Macromolecules*, *281*, 136201.
57. Nalini, Chadha, N., Bahia, M. S., Kaur, M., Bahadur, R., & Silakari, O. (2018). Computational design of new protein kinase D 1 (PKD1) inhibitors: homology-based active site prediction, energy-optimized pharmacophore, docking and database screening. *Molecular Diversity*, *22*, 47-56. https://link.springer.com/article/10.1007/s11030-017-9785-0.
58. Nwankwo, N. E., Egbuonu, A. C. C., Nduka, F. O., & Nwodo, O. F. C. (2017). Effect of seed extract of Picralima nitida on haematological parameters of malaria-infected albino mice and its interference with the serum electrolyte levels. *Ife Journal of Science*, *19*(2), 379-388. http://dx.doi.org/10.4314/ijs.v19i2.18.
59. Ochora, D. O., Kakudidi, E., Namukobe, J., Heydenreich, M., Coghi, P., Yang, L. J., ... & Yenesew, A. (2022). A new benzophenone, and the antiplasmodial activities of the constituents of Securidaca longipedunculata fresen (Polygalaceae). *Natural Product Research*, *36*(11), 2758-2766.
60. Okokon, J. E., Ettebong, E., & Antia, B. S. (2008). In vivo antimalarial activity of ethanolic leaf extract of Stachytarpheta cayennensis. *Indian journal of pharmacology*, *40*(3), 111-113. http://dx.doi.org/10.4103/0253-7613.42303.
61. Olawale, R. A. Malariology (A Continuing Education Activity)-2023 Revision. https://doi.org/10.31219/osf.io/zwr5q.
62. Onyeaghala, A. A., Anyiam, A. F., Husaini, D. C., Onyeaghala, E. O., & Obi, E. (2023). Herbal supplements as treatment options for COVID-19: a call for clinical development of herbal supplements for emerging and re-emerging viral threats in Sub-Saharan Africa. *Scientific African*, *20*, e01627.
63. Ouma, J. J. A. (2020). *A study of the antimalarial activity of combined plant extracts from medicinal plants used traditionally in Kenya* (Doctoral dissertation, University of Nairobi).
64. Patel, S. B. (2008). Plant sterols and stanols: their role in health and disease. *Journal of Clinical Lipidology*, *2*(2), S11-S19.

65. Perola, E., & Charifson, P. S. (2004). Conformational analysis of drug-like molecules bound to proteins: an extensive study of ligand reorganization upon binding. *Journal of medicinal chemistry*, *47*(10), 2499-2510.
66. Persch, E., Dumele, O., & Diederich, F. (2015). Molecular recognition in chemical and biological systems. *Angewandte Chemie International Edition*, 54(11), 3290-3327. https://doi.org/10.1002/anie.201408487.
67. Pinzi, L., & Rastelli, G. (2019). Molecular docking: shifting paradigms in drug discovery. *International Journal of Molecular Sciences*, *20*(18), 4331. https://doi.org/10.3390/ijms20184331.
68. Pitera, J. W. (2014). Expected distributions of root-mean-square positional deviations in proteins. *The journal of physical chemistry B*, *118*(24), 6526-6530.
69. Pulcini, S., Staines, H. M., Lee, A. H., Shafik, S. H., Bouyer, G., Moore, C. M., & Krishna, S. (2015). Mutations in the Plasmodium falciparum chloroquine resistance transporter, PfCRT, enlarge the parasite's food vacuole and alter drug sensitivities. *Scientific Reports*, *5*(1), 14552. https://doi.org/10.1038/srep14552.
70. Pulcini, S., Staines, H. M., Lee, A. H., Shafik, S. H., Bouyer, G., Moore, C. M., ... & Krishna, S. (2015). Mutations in the Plasmodium falciparum chloroquine resistance transporter, PfCRT, enlarge the parasite's food vacuole and alter drug sensitivities. *Scientific reports*, *5*(1), 14552.
71. Rayella, C., Devanandan, P., Rasuri, K., Yerravelly, S. S., Andem, S., & Puvvada, R. C. (2023). Clinical characteristics of malaria in COVID-19: A systematic review of case reports. *Tropical Parasitology*, *13*(1), 22-27.
72. Rehman, Y. U., Iqbal, A., Ali, G., Alotaibi, G., Ahmed, A., & Ayaz, M. (2024). Phytochemical analysis, radical scavenging and glioblastoma U87 cells toxicity studies of stem bark of buckthorn (Rhamnus pentapomica R. Parker). *BMC Complementary Medicine and Therapies*, *24*(1), 12. https://doi.org/10.1186/s12906-023-04309-w.
73. Ren, Y., & Kinghorn, A. D. (2020). Development of potential antitumor agents from the scaffolds of plant-derived terpenoid lactones. *Journal of medicinal chemistry*, *63*(24), 15410-15448.
74. Rotruck, J. T. ⍰., Pope, A. L., Ganther, H. E., Swanson, A. B., Hafeman, D. G., & Hoekstra, W. (1973). Selenium: biochemical role as a component of glutathione peroxidase. *Science*, *179*(4073), 588-590. https://doi.org/10.1126/science.179.4073.588.
75. Salaria, P., Subrahmanyeswara Rao, N. N., Dhameliya, T. M., & Amarendar Reddy, M. (2024). In silico investigation of potential phytoconstituents against ligand-and voltage-gated ion channels as antiepileptic agents. *3 Biotech*, *14*(4), 99.
76. Santa-María, C., López-Enríquez, S., Montserrat-de la Paz, S., Geniz, I., Reyes-Quiroz, M. E., Moreno, M., ... & Alba, G. (2023). Update on anti-inflammatory molecular mechanisms induced by oleic acid. *Nutrients*, *15*(1), 224.
77. Sedlak, J., & Lindsay, R. H. (1968). Estimation of total, protein-bound, and nonprotein sulfhydryl groups in tissue with Ellman's reagent. *Analytical biochemistry*, *25*, 192-205. https://doi.org/10.1016/0003-2697(68)90092-4.

78. Sharma, B., Legac, J., Cele, N., Awolade, P., Rosenthal, P. J., Singh, P., & Kumar, V. (2022). Functionalized 3-hydroxy-3-aminoquinoline-oxindole hybrids as promising dual-function anti-plasmodials. *European Journal of Medicinal Chemistry Reports*, *5*, 100052.
79. Sharma, J., Bhardwaj, V. K., Singh, R., Rajendran, V., Purohit, R., & Kumar, S. (2021). An in-silico evaluation of different bioactive molecules of tea for their inhibition potency against non structural protein-15 of SARS-CoV-2. *Food chemistry*, *346*, 128933.
80. Silva, D. A., Bowman, G. R., Sosa-Peinado, A., & Huang, X. (2011). A role for both conformational selection and induced fit in ligand binding by the LAO protein. *PLoS computational biology*, *7*(5), e1002054.
81. Singh, R., Bhardwaj, V., & Purohit, R. (2021). Identification of a novel binding mechanism of Quinoline based molecules with lactate dehydrogenase of Plasmodium falciparum. *Journal of Biomolecular Structure and Dynamics*, *39*(1), 348-356. https://doi.org/10.1080/07391102.2020.1711809.
82. Sinha, A. K. (1972). Colorimetric assay of catalase. *Analytical biochemistry*, *47*(2), 389-394. https://doi.org/10.1016/0003-2697(72)90132-7.
83. Small-Saunders, J. L., Hagenah, L. M., & Fidock, D. A. (2020). Turning the tide: targeting PfCRT to combat drug-resistant P. falciparum?. *Nature Reviews Microbiology*, *18*(5), 261-262.
84. Smith, D. A., Beaumont, K., Maurer, T. S., & Di, L. (2017). Relevance of half-life in drug design. *Journal of Medicinal Chemistry*, *61*(10), 4273-4282. https://doi.org/10.1021/acs.jmedchem.7b00969.
85. Soni, S., Tabatabaei Dakhili, S. A., Ussher, J. R., & Dyck, J. R. (2024). The therapeutic potential of ketones in cardiometabolic disease: impact on heart and skeletal muscle. *American Journal of Physiology-Cell Physiology*, *326*(2), C551-C566.
86. Sun, M., & Zigman, S. (1978). An improved spectrophotometric assay for superoxide dismutase based on epinephrine autoxidation. *Analytical biochemistry*, *90*(1), 81-89. https://doi.org/10.1016/0003-2697(78)90010-6.
87. Swierczewska, M., Lee, K. C., & Lee, S. (2015). What is the future of PEGylated therapies?. *Expert Opinion on Emerging Drugs*, *20*(4), 531-536. https://doi.org/10.1517/14728214.2015.1113254.
88. Tanner, J. D., Richards, S. N., & Corry, B. (2025). Molecular basis of the functional conflict between chloroquine and peptide transport in the Malaria parasite chloroquine resistance transporter PfCRT. *Nature Communications*, *16*(1), 2987.
89. Tarkang, P. A., Atchan, A. P. N., Kuiate, J. R., Okalebo, F. A., Guantai, A. N., & Agbor, G. A. (2013). Research Article Antioxidant Potential of a Polyherbal Antimalarial as an Indicator of Its Therapeutic Value. https://doi.org/10.1155/2013/678458.
90. Tran-Trung, H., Le, D. G., Hoang, V. T., Vu, D. C., Thang, T. D., Nguyen-Ngoc, H., ... & Nguyen, T. H. (2024). Essential oils of two species of Zingiberaceae family from Vietnam: chemical compositions and α-glucosidase, α-amylase inhibitory effects. *Natural Product Communications*, *19*(2), 1934578X241232281.
91. Vasa, V. K., Rao, T. M. V., Paturi, N., Penumatsa, K. V., & Haranadh, C. (2019). Liver dysfunction in malaria–An observational study. *IAIM*, *6*(4), 150-155.

92. Vasquez, M., Zuniga, M., & Rodriguez, A. (2021). Oxidative stress and pathogenesis in malaria. *Frontiers in cellular and infection microbiology*, *11*, 768182. https://doi.org/10.3389/fcimb.2021.768182.
93. Wang, E., Sun, H., Wang, J., Wang, Z., Liu, H., Zhang, J. Z., & Hou, T. (2019). End-point binding free energy calculation with MM/PBSA and MM/GBSA: strategies and applications in drug design. *Chemical reviews*, *119*(16), 9478-9508.
94. Wang, X., Shen, Y., Wang, S., Li, S., Zhang, W., Liu, X., & Li, H. (2017). PharmMapper 2017 update: a web server for potential drug target identification with a comprehensive target pharmacophore database. *Nucleic acids research*, *45*(W1), W356-W360. https://doi.org/10.1093/nar/gkx374.
95. Wicht, K. J., Mok, S., & Fidock, D. A. (2020). Molecular mechanisms of drug resistance in Plasmodium falciparum malaria. *Annual review of microbiology*, *74*, 431-454. https://doi.org/10.1146/annurev-micro-020518-115546.
96. Willcox, M., Bodeker, G., Rasoanaivo, P., & Addae-Kyereme, J. (2004). *Traditional medicinal plants and malaria*. CRC press. https://doi.org/10.1201/9780203502327.
97. Wink, M. (2015). Modes of action of herbal medicines and plant secondary metabolites. *Medicines*, *2*(3), 251-286. https://doi.org/10.3390/medicines2030251.
98. Wright, D. J., O'Reilly, M., & Tisi, D. (2018). Engineering and purification of a thermostable, high-yield, variant of PfCRT, the Plasmodium falciparum chloroquine resistance transporter. *Protein Expression and Purification*, *141*, 7-18.
99. Yang, S., & Kar, S. (2024). Protracted molecular dynamics and secondary structure introspection to identify dual-target inhibitors of Nipah virus exerting approved small molecules repurposing. *Scientific Reports*, *14*(1), 3696.
100. Zaveri, M. (2021). Bioactivity of Dodecanoic Acid Extracted from Geitlerinema sp. TRV57. *Indian Journal of Pharmaceutical Education & Research*, *55*(1). http://dx.doi.org/10.5530/ijper.55.1.25.
101. Zhao, M., Ma, J., Li, M., Zhang, Y., Jiang, B., Zhao, X., & Qin, S. (2021). Cytochrome P450 enzymes and drug metabolism in humans. *International Journal of Molecular Sciences*, *22*(23), 12808. https://doi.org/10.3390/ijms222312808.

Figures

Figure 1

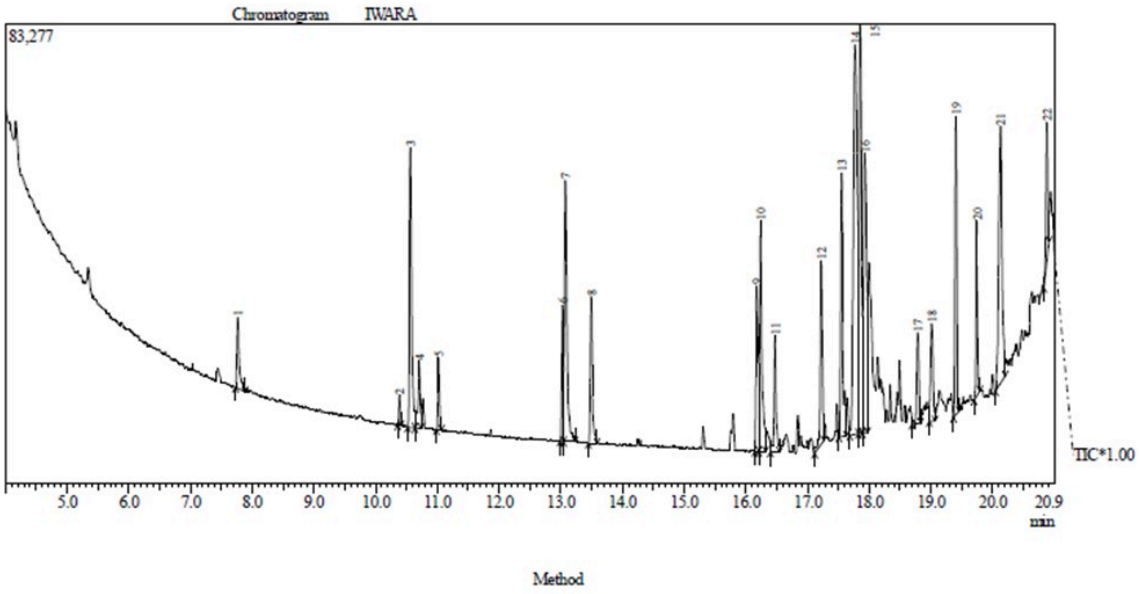

Figure 1

Chromatogram of polyherbal extract of Garlic, Ginger, and Turmeric

Figure 2

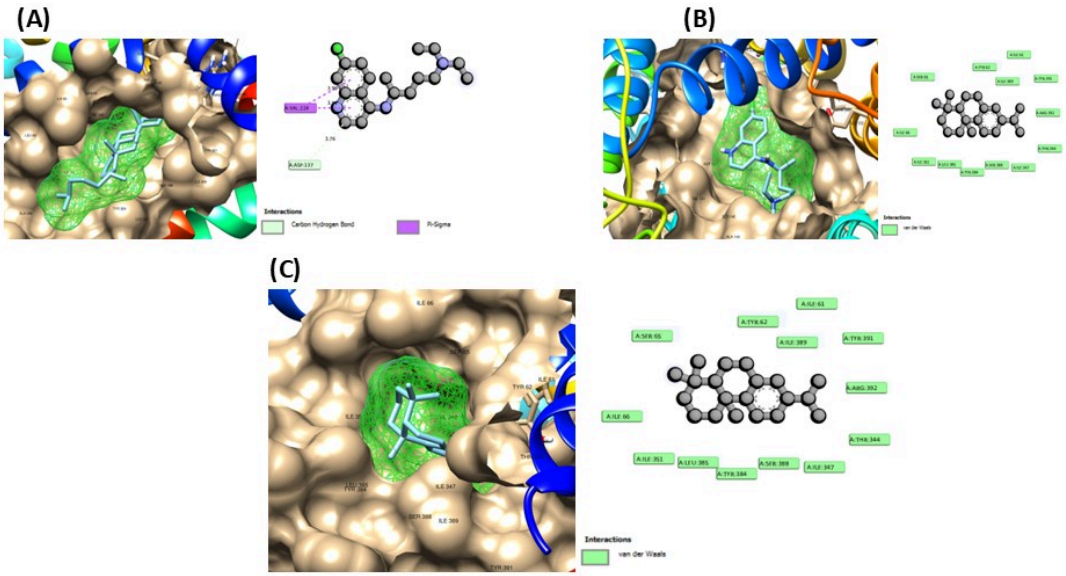

Figure 2

A-D: 3D (left) and 2D (right) views of the molecular interactions of amino-acid residues of Chloroquine resistance transporter: chloroquine (A) Cholest-14-en-3-ol, (3.beta.,5.alpha.)(B) 7-Isopropyl-1,1,4a-trimethyl-1,2,3,4,4a,9,10,10a-octahydrophenanthrene(C)

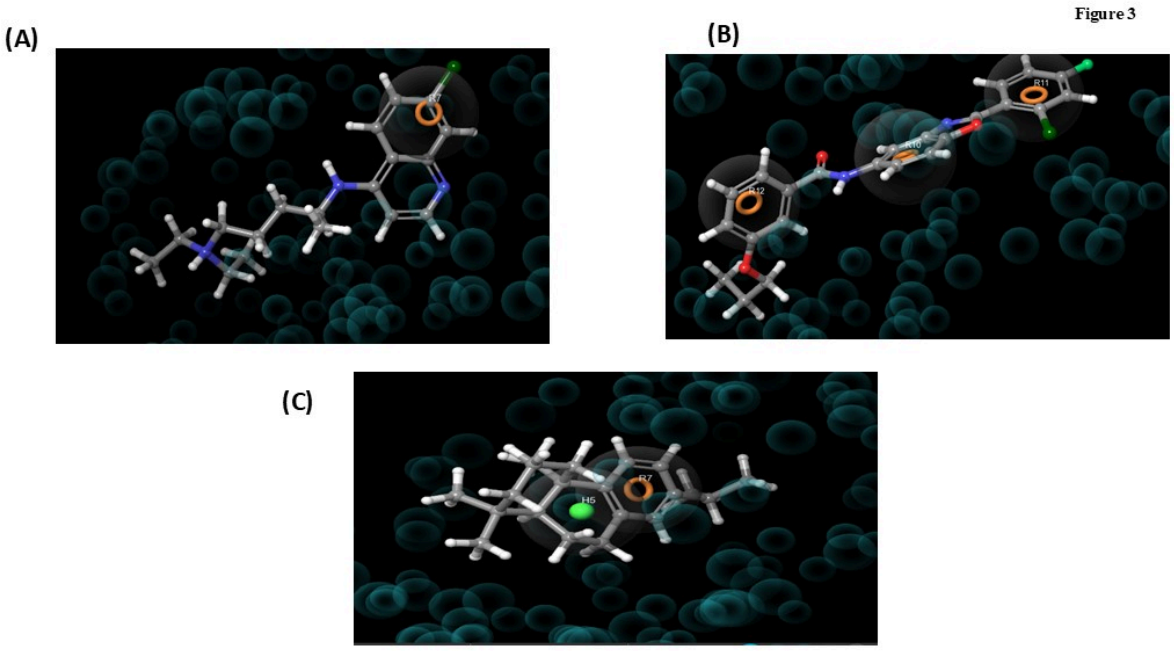

Figure 3

A-D: Pharmacophore model of the molecular interactions of amino-acid residues of Chloroquine resistance transporter: chloroquine (A)Cholest-14-en-3-ol, (3.beta.,5.alpha.)(B) 7-Isopropyl-1,1,4a-trimethyl-1,2,3,4,4a,9,10,10a-octahydrophenanthrene

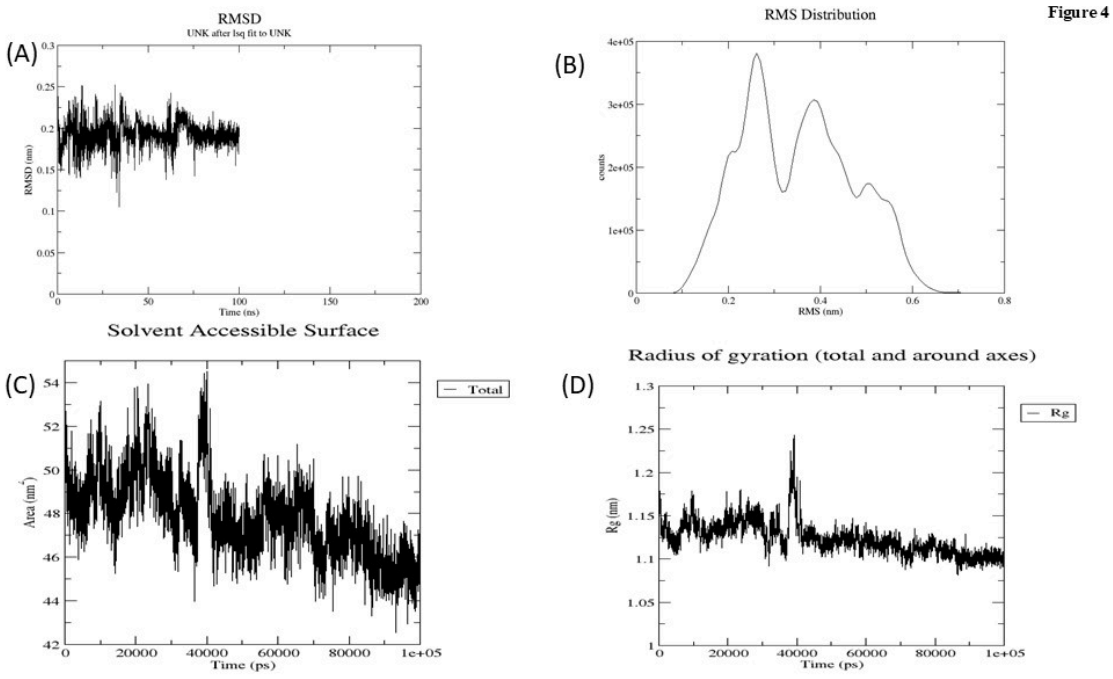

Figure 4

Root Mean Square Deviations (RMSD: A), root mean square distribution (RMSD: B), solvent accessible surface area (SASA: C); radius of gyration (Rg: D) of Chloroquine resistance transporter(*PfCRT)* with Cholest-14-en-3-ol, (3.beta.,5.alpha.)-

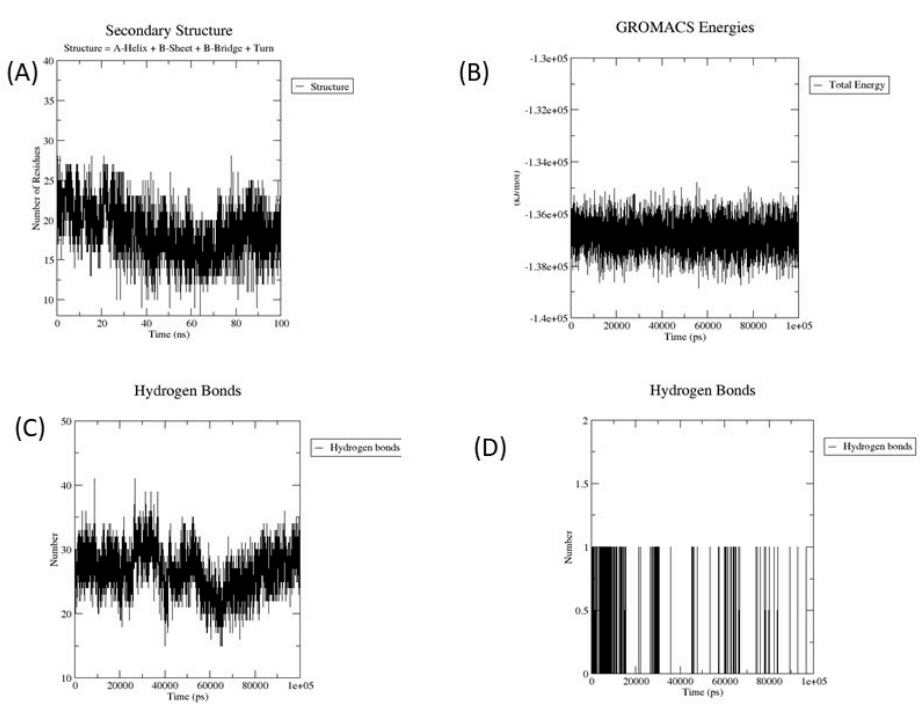

Figure 5

Secondary structure (A); Gromacs energy (B); Protein-Ligand Hydrogen bonds (H-Bonds: C) Protein Hydrogen bond (D) of Chloroquine resistance transporter(*PfCRT)* with Cholest-14-en-3-ol, (3.beta.,5.alpha.)-

Figure 6

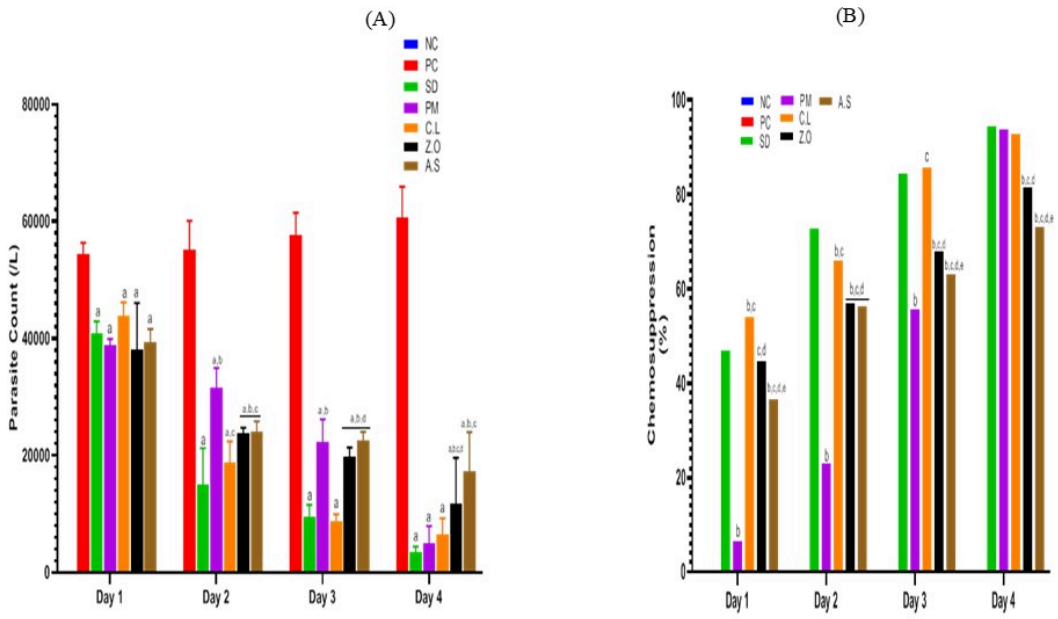

Figure 6

Malaria parasite density(A) and chemosuppression of malaria parasite(B) in the different experimental groups. Data are given as mean ± standard error of the mean (SEM) of n = 8. Different letters (a, b, c and d) denote significant difference between treated groups at $p < 0.05$

Figure 7

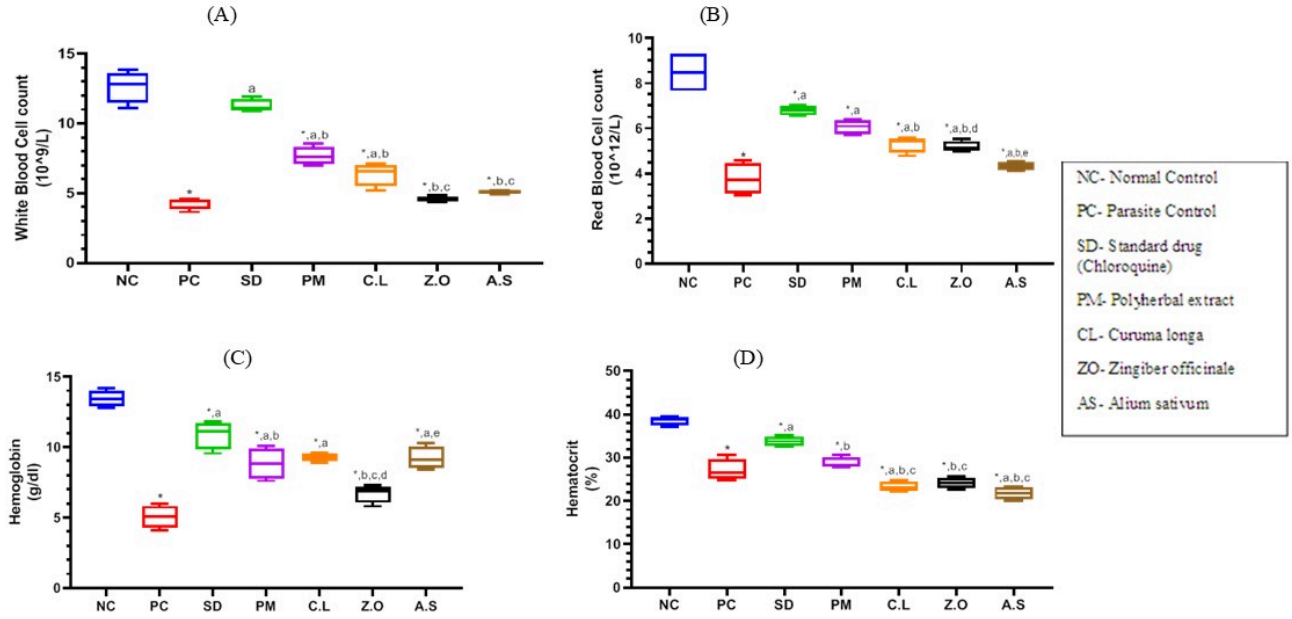

Figure 7

A-D: WBC and RBC Counts, Hb Concentration and PCV in the experimental groups. Data are given as mean ± standard error of the mean (SEM) of n = 8. Different letters (*, a, b, c and d) denote significant difference between treated groups at $p < 0.05$

Figure 8

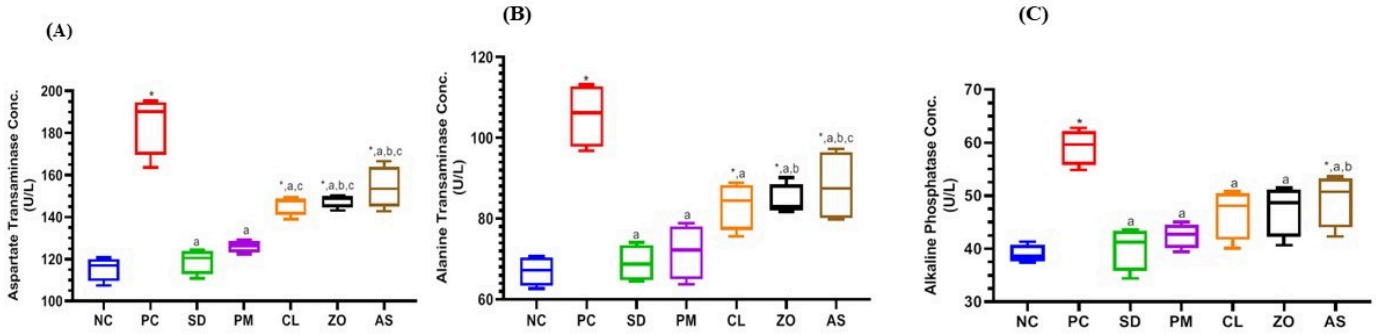

Figure 8

A-D: Liver enzyme parameters in the experimental groups. Data are given as mean ± standard error of the mean (SEM) of n = 8. Different letters (*, a, b, c and d) denote significant difference between treated

groups at p < 0.05.

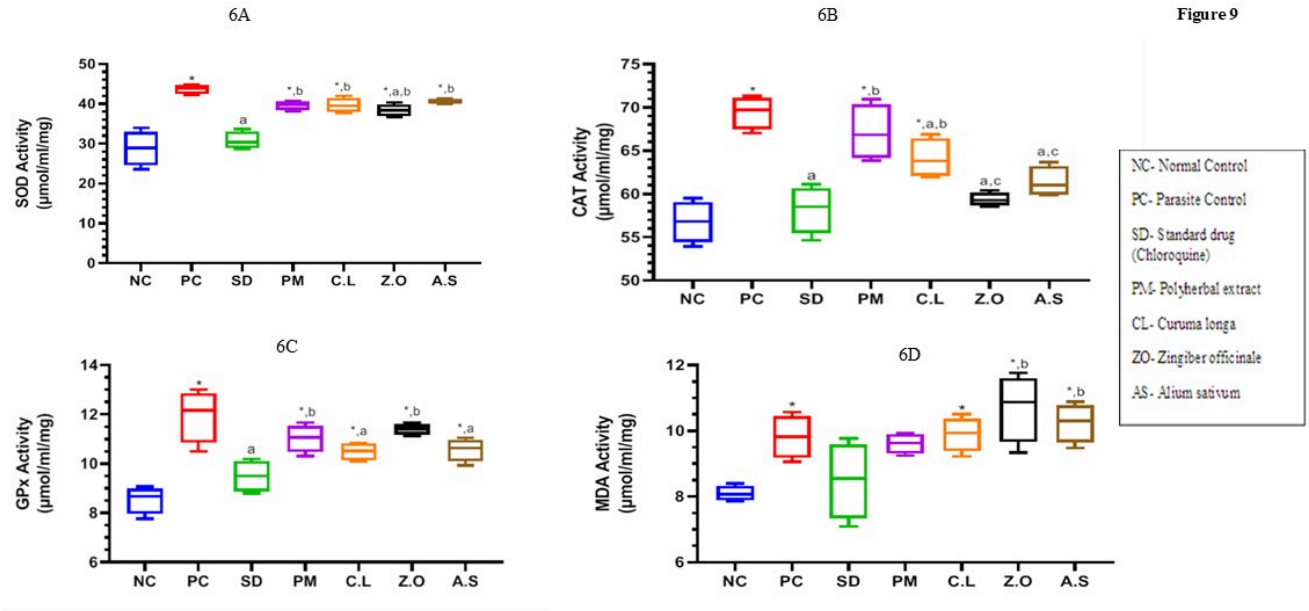

Figure 9

A-D showing Antioxidant and Oxidative stress enzymes activity in the experimental groups. Data are given as mean ± standard error of the mean (SEM) of n = 8. Different letters (*, a, b, c and d) denote significant difference between treated groups at p < 0.05